MAPPING AUDITORY NERVE FIRING DENSITY USING THE COMPOUND ACTION POTENTIAL AND HIGH-PASS NOISE MASKING

BY

Brian R. Earl, M.S., CCC-A

Submitted to the Intercampus Program in Communicative Disorders and the Graduate Faculty of the University of Kansas in partial fulfillment of the requirements for the degree of Doctor of Philosophy.

_____
Mark E. Chertoff, PhD, Chairperson

_____
John A. Ferraro, PhD, Committee Member

_____
Judith E. Widen, PhD, Committee Member

_____
Tiffany A. Johnson, PhD, Committee Member

_____
Thomas J. Imig, PhD, Committee Member

Date defended: September 1, 2010

The Dissertation Committee for Brian R. Earl certifies that
this is the approved version of the following dissertation:

MAPPING AUDITORY NERVE FIRING DENSITY USING THE COMPOUND ACTION POTENTIAL AND HIGH-PASS NOISE MASKING

Committee:

_____
Mark E. Chertoff, PhD, Chairperson

_____
John A. Ferraro, PhD, Committee Member

_____
Judith E. Widen, PhD, Committee Member

_____
Tiffany A. Johnson, PhD, Committee Member

_____
Thomas J. Imig, PhD, Committee Member

Date approved: September 1, 2010

ACKNOWLEDGEMENTS

I express my sincere gratitude to Dr. Mark E. Chertoff for his exceptional mentoring in the classroom, the lab, and life. Our conservations about the ups and downs of parenting have been just as valuable as our chalkboard discussions about the ups and downs of the wave equation. His unassuming "How do I know I'm right?" motto for problem-solving, even after applying extensive thought and careful logic, is a motto I hope to emulate. I also express thanks to Dr. John A. Ferraro, Dr. Judith E. Widen, Dr. Tiffany A. Johnson, and Dr. Thomas J. Imig for their contributions to this project and their willingness to serve as members of my committee.

Dedication

To my wife, Marilin, and to my children, Maya, Merica, Aaron, Colby, and Eric, for their continual support and encouragement.

ABSTRACT

A critical barrier to future implementation of regenerative treatments for sensorineural hearing loss is the lack of diagnostic tools that can specify the target(s) within the cochlea and auditory nerve for delivery of therapeutic agents. This study used a gerbil model to test the idea of mapping auditory nerve firing density by tracking the amplitude of high-level compound action potentials (CAPs) while varying the bandwidth of simultaneous masking noise. The distributions of neural firing, obtained by calculating the derivative of the equation describing CAP amplitude growth as a function of distance along the cochlea, indicated that high-level chirp stimuli trigger widespread neural firing in the cochlea that is unaltered by sensory outer hair cell pathology. These results suggest that CAP-derived neural density functions for high-level chirp stimuli may provide reliable maps of auditory nerve density in impaired ears.

TABLE OF CONTENTS

COMMITTEE APPROVAL ii

ACKNOWLEDGEMENTS iii

DEDICATION iv

ABSTRACT v

INTRODUCTION 1

MATERIALS AND METHODS 5

Animal Preparation 5

Generation of CAP Stimuli and Masking Noise 5

CAP Recordings 7

Procedures 7

Data Analysis 10

RESULTS 12

Unmasked CAP Amplitudes 12

Experiment 1: Cumulative Amplitude Functions (CAFs) 13

Experiment 1: Neural Density Functions (NDFs) 14

Experiment 2: Gentamicin-Induced Changes in CM Amplitude and CAP Threshold 15

Experiment 2: CAF & NDF Comparisons across Groups 16

Experiment 2: Variability in NDF Peak Location 17

DISCUSSION 17

Experiment 1: NDF Differences across Stimulus Type 18

Experiment 2: NDF Comparisons across Groups 18

Unmasked CAP Amplitudes 19

CAP Latency Shifts 20

Chirp Stimulus 20

High-Pass Noise Masking Paradigm 21
Sigmoid Model Performance 22
Alternative Method of Analysis 22
Future Directions 23
CONCLUSIONS 24
REFERENCES 25
APPENDIX A. Literature Review 35
Introduction 36
Auditory Nerve Degeneration 36
Influence of Stimulus Characteristics on AEPs 39
Masked AEPs 42
Gentamicin-Induced Impairment of OHCs 45
Influence of OHC Pathology on High-Level AEPs 48
APPENDIX B. Figures and Tables 50
Figure 1 51
Figure 2 52
Figure 3 53
Figure 4 54
Figure 5 55
Figure 6 56
Figure 7 57
Figure 8 58
Figure 9 59
Figure 10 60
Figure 11 61

Table 1 62

Table 2 63

APPENDIX C. CAP Waveforms 64

Figure C.1 65

Figure C.2 66

Figure C.3 67

Figure C.4 68

Figure C.5 69

Figure C.6 70

APPENDIX D. Latency Analysis 71

Figure D.1 72

Figure D.2 73

APPENDIX E. Alternate Analysis Method 74

Figure E.1 75

INTRODUCTION

Prompt diagnosis and treatment of hearing loss can avert delays in speech and language acquisition in children (Yoshinaga-Itano et al., 1998; Moeller, 2000; Cunningham and Cox, 2003) and social isolation in adults (Monzani et al., 2008; Poissant et al., 2008). The development of objective diagnostic tools such as auditory evoked potentials (AEPs) and otoacoustic emissions (OAEs) has significantly reduced the age of identification of hearing loss in children (Cone-Wesson et al., 2000) and enhanced differentiation of the sensory and neural components of sensorineural hearing loss. Advances in hearing aid and cochlear implant technology have resulted in modest improvements in word recognition performance (Koch, 2004; Bentler et al., 2006; Firszt, 2009), listening comfort in noise (Chung et al., 2006; Bentler et al., 2008), and patient satisfaction (Kochkin, 2007; Ou et al., 2008). Yet benefit from even the most advanced technology can vary considerably across patients with similar audiometric profiles suggesting differences in the underlying pathology that are not apparent in routine clinical measures of hearing impairment. Advanced diagnostic techniques that can pinpoint the cochlear location of hair cell loss and neural degeneration may improve individualization of gain prescriptions for hearing aids and offer guidance for optimal electrode positioning (Briaire and Frijns, 2006) and mapping strategies for cochlear implant recipients (Bierer and Faulkner, 2010). Such precise diagnostic tools would also seem to be crucial if cochlear hair cell regeneration (e.g., Edge and Chen, 2008) and auditory nerve regeneration (e.g., Matsuoka et al., 2007; Agterberg et al., 2009) eventually become viable treatment options for individuals with sensorineural hearing loss.

Since OAEs and short-latency AEPs reflect cochlear outer hair cell (OHC) and auditory nerve function, respectively, they likely offer the best non-invasive glimpse of peripheral pathophysiology contributing to sensorineural hearing loss. Presence or absence of OAEs and threshold and latency of AEPs are the parameters routinely analyzed in the clinic. However, analysis of other response parameters such as amplitude, response area, and morphology may expand the diagnostic utility of these measures. For example, Don et al. (2005) demonstrated that their stacked auditory brainstem response (ABR)

technique, which optimizes wave V amplitude by temporally aligning and summing derived-band ABRs, detects the presence of small acoustic neuromas with 95% sensitivity and 88% specificity. Ferraro and Durrant's (2006) method of calculating the area ratio between the summating potential (SP) and the action potential (AP) portions of electrocochleography waveforms achieves 92% sensitivity and 84% specificity in diagnosing Ménière's disease/endolymphatic hydrops (Al-momani et al., 2009). Other studies in the cochlear implant literature have indicated that the amplitude of electrically evoked auditory potentials is positively correlated with the number of viable auditory neurons (Smith and Simmons, 1983; Hall, 1990) and may predict prognosis for implant recipients (Gibson and Sanli, 2007; Teagle et al., 2010).

Chertoff (2004) and Chertoff et al. (2008) used a gerbil model to investigate the utility of the compound action potential (CAP) in identifying auditory nerve fiber degeneration. Their approach was to quantify the morphology of CAPs by fitting the waveforms with a five-parameter convolution model adapted from Goldstein and Kiang (1958). One of the model parameters (*N*) scales the magnitude of the N_1 portion of the CAP similar to conventional measures of N_1 amplitude (i.e., baseline to N_1 peak) and theoretically represents the number of nerve fibers contributing to the recorded response. Earl and Chertoff (2010) tested this theory by using the convolution model to fit CAPs evoked with tonebursts (1-16 kHz) in gerbils with partial lesions of the auditory nerve. At high stimulus levels (100 dB SPL for 1-8 kHz, 75 dB SPL for 16 kHz), the model parameter *N* and conventional measures of N_1 amplitude were positively correlated with the percentage of surviving nerve fibers within the whole nerve bundle. Although the measures of N_1 magnitude of high-level CAPs appeared to predict overall auditory nerve survival, the magnitude values at different stimulus frequencies did not pinpoint the corresponding frequency region of the cochlea where neural damage was located.

A location-specific estimate of neural damage may be possible by systematically limiting the region of nerve fibers contributing to high-level CAPs with a high-pass noise masking paradigm (e.g., Bone et al., 1972; Shore and Nuttall, 1985; see Literature Review in Appendix A). The schematic of an

uncoiled cochlea and the accompanying plots in Figure 1 illustrate the theory behind the idea. A high-level stimulus that triggers synchronous neural excitation along the majority of the cochlea is used to evoke CAPs while the high-pass cutoff frequency of simultaneous masking noise is stepped from low frequencies encoded in the apex to high frequencies encoded in the base. In a normal cochlea with a full complement of nerve fibers, normalized N_1 amplitude accumulates in a sigmoid manner as progressively more neurons are allowed to contribute to the CAP (solid line in Figure 1, bottom left panel). Plotting the derivative of the cumulative amplitude function yields a neural density function that is assumed to represent the spread of neural firing generated in the cochlea by a given stimulus (solid line in Figure 1, bottom right panel). In a cochlea with a gap of missing auditory nerve fibers (dashed line in Figure 1, bottom left panel), normalized N_1 amplitude would increase faster than normal until the masker cutoff frequency moves into the region of missing nerve fibers. Since there are no additional nerve fibers to contribute to the CAP, the amplitude function would plateau until the masker moves more basally to the location where nerve fibers are present. The neural density function for the cochlea with missing fibers (dashed line in Figure 1, bottom right panel) would show a drop in neural firing density that is assumed to identify the distance along the basilar membrane where neurons are nonfunctional or absent (Figure 1, bottom right panel).

The long-term goal of this research is to test the theory that CAP-derived neural density functions can predict the corresponding cochlear location of auditory nerve degeneration in impaired ears. The objective of this study was to use the high-pass masking technique to answer the following two questions that are pertinent to achieving the long-term goal:

1. What is the ideal acoustic stimulus for evoking synchronous neural firing along the majority of the cochlea?
2. Does OHC pathology alter high-level neural density functions?

To answer the first question, two types of acoustic stimuli were considered. According to the traveling wave theory, a high-level low frequency toneburst may be ideal because it triggers substantial

basilar membrane displacement from the base of the cochlea to the characteristic low frequency place in the apex (Eggermont, 1976). A rising frequency toneburst (i.e., chirp) may be more ideal than a low frequency toneburst because the high frequency components of a chirp are delayed relative to the low frequency components which compensates for the cochlear traveling wave delay. This temporal compensation theoretically leads to simultaneous displacement and synchronous neural firing along the majority of the basilar membrane (Shore and Nuttall, 1985; see Literature Review in Appendix A).

The findings of several studies on the influence of stimulus level on cochlear mechanics suggest the answer to the second question. Specifically, the findings of Dallos and Harris (1978), Ruggero and Rich (1991), and Fridberger et al. (2002) indicate that OHCs act primarily to enhance basilar membrane displacement for low to moderate-level inputs. High-level inputs (e.g., 90 dB SPL) are assumed to trigger sufficient basilar membrane displacement to stimulate the inner hair cells (IHCs) directly. Therefore, any changes in high-level neural density functions would not be related to OHC pathology but would reflect the status of the primary afferent neurons that synapse with IHCs. Neural density functions for moderate-level stimuli (e.g., 60 dB SPL) would be expected to be influenced by OHC pathology.

Consideration of these theories and experimental observations led to the formulation of the following hypotheses for this study:

1. High-level chirps trigger a broader spread of synchronous neural firing along the cochlear partition than high-level low frequency tonebursts.
2. OHC pathology does not alter high-level neural density functions.

The first hypothesis was tested in normal-hearing gerbils (Experiment 1) by comparing neural density functions obtained for chirps and for 2 kHz (relatively low frequency for gerbil) tonebursts. The second hypothesis was tested in an additional experiment (Experiment 2) by comparing neural density functions obtained from gentamicin-exposed gerbils to those obtained from normal-hearing gerbils in Experiment 1.

Materials and Methods

Animal Preparation

Young-adult Mongolian gerbils (Meriones unguiculates), weighing between 45 and 70 grams, were used for this study. A gerbil model is ideal because their low frequency hearing sensitivity is similar to that of the human auditory system and due to the ease of the surgical approach to the cochlea. Prior to surgery, all animals were sedated with an initial intraperitoneal injection of pentobarbital (64 mg/kg). Supplementary intramuscular injections of pentobarbital (~30 mg/kg) were given hourly to maintain appropriate sedation throughout the surgery and data collection. Animals were placed in the supine position and wrapped in a warming pad to maintain body temperature at 37^{o} C. Following local injection of lidocaine, a 10-15 mm post-auricular incision was made and the underlying neck musculature was dissected to access the right middle ear cavity (bulla). The bulla was opened with surgical tweezers to allow for placement of an electrode in the round window niche for CAP recordings (Experiments 1 and 2) and delivery of gentamicin solution to the niche to induce OHC impairment (Experiment 2). All experimental procedures were approved by the Institutional Animal Care and Use Committee of the University of Kansas Medical Center.

Generation of CAP Stimuli and Masking Noise

A gerbil-tailored chirp stimulus and a traditional 2 kHz toneburst stimulus were generated for this study. The chirp stimulus (Fig. 2, left panel) was tailored to gerbil by sweeping the frequency from 1 to 60 kHz, nearly the entire frequency range of gerbil hearing, at a rate that coincides with the inverse of an estimate of cochlear traveling wave delay in gerbil (Fig.2, middle panel). The cochlear traveling wave delay was estimated by fitting gerbil CAP latency data for toneburst stimuli between 1 and 16 kHz at 5 dB above threshold (Earl and Chertofff, 2010) with the following equation:

$$t(f) = cf^{\alpha} \qquad (1)$$

where *t(f)* is cochlear traveling wave delay in seconds (s), *f* is stimulus frequency in Hz, and the constants *c* and α are 0.01415 and -0.1960, respectively. Using these constants and equations 3-6 of Fobel and Dau (2004), the chirp waveform was generated in Matlab (MathWorks, Natick, MA) using a time resolution of 4 μs (i.e., sampling frequency = 250 kHz). Ramping up the amplitude of the chirp stimulus (Fig. 2, left panel) as the instantaneous frequency increased, according to the amplitude scaling factor (Eq. 7) of Fobel and Dau (2004), produced a chirp with relatively flat spectral magnitude between 1 and 60 kHz (Fig. 2, right panel). Chirp stimuli were presented with alternating polarity at a rate of 25/s.

A traditional 2 kHz toneburst stimulus was generated with 1 ms rise/fall times and an 8 ms plateau. A relatively long-duration toneburst (e.g., 10 ms) was chosen to facilitate differentiation of the N_1 and SP components of the CAP. Tonebursts were delivered with alternating polarity, to minimize the cochlear microphonic (CM), at a rate of 40/s.

Broadband white noise was generated (D/A sampling rate = 97.7 kHz) and high-pass filtered with fifth order Butterworth filters (slopes ≥ 80 dB per octave) using signal processing software (RPvdsEx) and a Real-time Processor (RP2) from Tucker-Davis Technologies (TDT; Alachua, FL, USA). Multiple high-pass cutoff frequencies were chosen to correspond to 0.25 mm increments along the first 3 mm of the base of the gerbil cochlea where the best frequency ranges from 53.4 kHz to 13.8 kHz. For the middle through apical regions of the gerbil cochlea (3-11 mm), where the best frequency ranges from 13.2 kHz to 360 Hz, cutoff frequencies were chosen to correspond to 0.5 mm increments. The lowest cutoff frequency was 400 Hz and the highest cutoff frequency was 45987 Hz making a total of 25 masking conditions. Since the spectral energy of white noise decreases as the spectral bandwidth decreases (i.e., high-pass cutoff frequency increases), the root-mean-square (RMS) SPL of the partial-bandwidth masking conditions were equated to the RMS SPL of the full-bandwidth masking condition (0.4-50 kHz). Otherwise, changes in spectral energy of the noise across masking conditions could confound the interpretation of CAP amplitude changes.

The masking signal was added to the CAP stimulus (i.e., chirp or 2 kHz toneburst) with a signal mixer (SM5, TDT) and delivered via a magnetic loudspeaker (FF1, TDT) with a relatively flat (+/- 8 dB) frequency response from 1 to 50 kHz. Electromagnetic artifact from the loudspeaker was minimized to negligible levels by housing the loudspeaker in a custom-made mu metal case (MμShield; Manchester, NH, USA) and by positioning it 15 cm away from the opening of the animals' ear canals. A 1/8" Brüel & Kjaer (Denmark) microphone (B&K 4138) was suspended within 5 mm and at a 90 degree azimuth relative to the ear canal opening and diaphragm of the loudspeaker. The reported frequency sensitivity of the B&K microphone is essentially flat (+/- 2 dB) from 0.02 to 100 kHz when it is positioned at a 90 degree azimuth relative to the sound source. The microphone output was routed to an oscilloscope and a spectrum analyzer; the oscilloscope (Tektronix, TDS 2014) to calibrate the peak SPL (pSPL) of the CAP stimulus (i.e., chirp or 2 kHz toneburst), and the spectrum analyzer (Hewlett Packard, 3561A) to verify the spectral bandwidth of each masking condition.

CAP Recordings

CAPs were recorded using a silver ball electrode on the round window and a ground electrode in the contralateral shoulder musculature. An absorbent cotton wick (Densply Maillefer, Tulsa, OK) was placed next to the round-window electrode and subsequently changed every 15 minutes to control fluid build-up in the niche. The electrophysiologic signals were amplified by a factor of 5000, band-pass filtered (0.03- 6 kHz) by two amplifiers/filters in series (Stanford Research Systems SR560, Sunnyvale, CA, USA; Stewart Electronics VBF10, Lyman, SC, USA), and digitized at 250 kHz by an analog to digital converter (AD2, TDT) before being averaged within a 15 ms time window. The raw CAP waveforms were named according to stimulus type, stimulus level, and high-pass cutoff frequency, and then saved to disk after sufficient averages were obtained to achieve an adequate signal to noise ratio.

Procedures

In Experiment 1, data were collected from a group of normal-hearing gerbils (n=9) to compare neural density functions for chirps and 2 kHz tonebursts at a high level (90 dB pSPL) and at a moderate

level (60 dB pSPL). Animals were considered to have normal hearing sensitivity if their CAP threshold for chirps was ≤ 20 dB pSPL. N_1 amplitude growth data was obtained for the four stimulus conditions in the following order: chirps at 60 dB pSPL, 2 kHz tonebursts at 60 dB pSPL, chirps at 90 dB pSPL, and 2 kHz tonebursts at 90 dB pSPL. Each recording condition began by measuring the amplitude of N_1 (baseline to negative peak of N_1 as demonstrated in Fig. 3, left panel) of the unmasked CAP on a digital oscilloscope (Tektronix TDS 2014). The full-bandwidth masker (0.4-50 kHz) was then presented and attenuated to a level that reduced the amplitude of N_1 by 80% similar to the procedure of Eggermont (1977). The bandwidth of the white noise was subsequently varied by changing the high-pass cutoff frequency and CAPs were recorded for each of the 25 masking conditions. The sequence of masking conditions was randomized and interspersed with two recordings of unmasked CAPs. A fourth unmasked CAP was recorded after all masking conditions were presented. Representative unmasked and masked CAPs for six different stimulus conditions are presented in Appendix C. The average time required to record the 29 CAPs for one stimulus condition was 27 minutes while the average duration of the entire protocol of Experiment 1 was just over 2 hours. The CAP threshold for chirps was measured again at the completion of the protocol to determine if the multiple presentations of masking noise led to an elevation in threshold.

In Experiment 2, data were collected from a group of gentamicin-exposed gerbils (n=10) to compare neural density functions obtained from animals with impaired OHCs to the neural density functions obtained from the normal-hearing gerbils in Experiment 1. Gentamicin, an aminoglycoside antibiotic, was chosen for this study based on data from several studies indicating that OHCs are more prone to gentamicin ototoxicity than are IHCs (e.g., Wanamaker et al., 1998; Heydt et al., 2004; see Literature Review in Appendix A). The chosen dosage of gentamicin (200 µg applied directly to round window) was based on data for mice (Heydt et al., 2004) and gerbils (Wanamaker et al., 1998; Sheppard et al., 2004; Suryadevara et al., 2009) showing that similar dosages led to OHC pathology across the base to middle regions of the cochlea. A 200 µg/µl gentamicin solution was prepared by dissolving

gentamicin sulfate powder (Sigma; St. Louis, MO, USA) in distilled water after the manner described by Husmann et al. (1998). Specifically, to achieve a 200 µg/µl (i.e., 200 mg/ml) concentration of gentamicin in solution, 313 mg of gentamicin sulfate powder, containing 0.639 mg of gentamicin per mg, was dissolved in 1 ml of distilled water.

Prior to gentamicin exposure, baseline CAP thresholds were determined for chirps and toneburst stimuli at 2, 4, 8, 16, and 32 kHz. The amplitude of the cochlear microphonic (CM) to a 16 kHz toneburst (10 ms duration) at 80 dB pSPL was also measured prior to gentamicin delivery and then monitored during the exposure period to gauge the effect of gentamicin on OHC function. The CM recordings were acquired with the same electrode montage, recording parameters, and instrumentation set-up as the CAP recordings with one exception: the low-pass filter setting was changed from 6 kHz to 25 kHz to capture the CM to the 16 kHz tone. A high frequency tone (e.g., 16 kHz) was chosen for CM monitoring under the assumption that it would provide an early indication of OHC impairment resulting from the diffusion of gentamicin through the round window membrane and into the basal region (i.e., high frequency region) of the cochlea (Wanamaker et al., 1998). Without removing the recording electrode, 1 µl of the 200 µg/µl gentamicin solution was applied directly to the round window niche. The amplitude of the CM was monitored 1 minute post-gentamicin application and then in 5-minute increments until the CM amplitude had dropped by at least 50% (relative to the pre-gentamicin amplitude) and at least 15 minutes had elapsed. The gentamicin solution was then removed from the niche with an absorbent cotton wick and the CAP threshold to chirps was measured again. If the chirp CAP threshold had increased by at least 10 dB, the experiment proceeded with post-gentamicin measures of N_1 amplitude growth for chirps at 60 dB pSPL and then for chirps at 90 dB pSPL using the same masking procedures described above. Masked CAPs were not recorded for 2 kHz tonebursts at 60 or 90 dB pSPL per the results of Experiment 1 (see below). The chirp CAP threshold and toneburst CAP thresholds were measured again following the completion of both stimulus conditions. The average time required for one stimulus condition in

Experiment 2 was 23 minutes and the average duration of the entire masked CAP protocol was 52 minutes.

Data Analysis

Manual measures of N_1 peak amplitude (baseline to N_1 peak) and N_1 peak latency for all stimulus conditions of both experiments were completed offline in Matlab following data collection. The left panel of Figure 3 displays representative unmasked and masked CAPs indicating the trend, observed in this and other studies (e.g. Teas et al., 1962; Shore and Nuttall, 1985), of decreasing N_1 amplitude and increasing N_1 latency as high-pass masker cutoff frequency decreases. The raw amplitude values (filled circles, Fig. 3, right panel) were normalized relative to the average unmasked amplitude to allow for amplitude growth comparisons across stimulus types and levels. The raw latency values (open circles, Fig. 3, right panel) were also normalized by calculating the shift in latency by subtracting the average unmasked latency from the masked latency.

Figure 4 demonstrates the data-fitting procedure (left panel) and the two dependent variables used for statistical analyses (right panel). First, normalized N_1 amplitude values for the masked CAPs were plotted as a function of distance from apex in mm (Fig. 4, left panel). The high-pass cutoff frequencies (as shown on the abscissa in Fig. 3, right panel) were converted to distance from apex in mm (as shown on the abscissa in Fig. 4, left panel) using the frequency-place map for gerbil cochleae from Müller (1996). The cumulative amplitude function (CAF; thick curve in Fig. 4, left panel) was obtained for each stimulus condition by using SigmaPlot (Systat Software, Inc., San Jose, CA, USA) to fit the normalized N_1 amplitude data with the following four-parameter sigmoid function:

$$CAF(x) = y_0 + \left(\frac{a}{1 + e^{-\left(\frac{x - x0}{b}\right)}} \right) \qquad (2)$$

where *a* scales the inflection point of N_1 amplitude growth, *b* governs the rate of amplitude growth, *x0* is the distance from apex (mm) where inflection of amplitude growth occurs, and *y0* defines the starting amplitude reduction relative to the unmasked amplitude. The parameter *y0* is a constant in terms of Eq. 2 and in the design of the masking paradigm since the target level for the initial masked condition was 20% of the unmasked amplitude. The neural density function (NDF; thick curve in Fig. 4, right panel) was obtained for each stimulus condition by using the CAF parameters to solve the analytical derivative of Eq. 2 for distance from apex (*x*) which is:

$$NDF(x) = \left(\frac{ae^{\left(\frac{x0+x}{b}\right)}}{b(e^{\left(\frac{x0}{b}\right)} + e^{\left(\frac{x}{b}\right)})^2} \right) \qquad (3)$$

where *a* and *b* proportionally scale the peak density and bandwidth, respectively, and *x0* is the peak location in distance from apex (mm).

The theoretical foundation for constructing NDFs by taking the derivative of CAFs is based on the relationship between two functions that are pertinent to probability theory: the cumulative distribution function and the probability density function (Feller, 1968). The cumulative distribution function is an s-shaped curve spanning negative to positive values across the x-axis as it grows steadily from 0 to 1 on the y-axis. Plotting the derivative of the cumulative distribution function yields the probability density function, a bell-shaped curve spanning the same negative to positive values across the x-axis and peaking on the y-axis where x = 0. The N_1 amplitude growth functions that were generated with the high-pass masking paradigm in this study are not only similar in appearance to the s-shaped cumulative distribution function but are also similar in construction. In other words, the N_1 amplitude growth function represents an accumulation of amplitude as progressively more neurons are allowed to synchronously contribute to the CAP as the cochlear spread of the masker decreases. Given this foundation and amplitude growth functions with 25-point resolution, it seems reasonable to use sigmoid functions (of similar form as the

cumulative distribution function) to fit the amplitude data and take the analytical derivative of that equation (i.e., CAF) to construct the NDF.

The two dependent variables chosen for statistical analysis (SPSS 17.0) were NDF bandwidth and NDF peak location. NDF bandwidth quantifies the cochlear spread of synchronous neural firing and NDF peak location identifies the location along the cochlear partition where neural firing density peaks. NDF bandwidth was defined as the distance spanned by the inner 2/3 of the area under the NDF curve and was calculated by multiplying the peak density of the NDF by 0.3413 and finding the difference between the corresponding values for distance from apex. NDF peak location was given by the value of parameter *x0*. Paired samples t-tests were used to compare bandwidth and peak location across stimulus type at 60 and 90 dB pSPL in Experiment 1. Independent samples t-tests were used to compare bandwidth and peak location of chirp-generated NDFs across the normal-hearing and gentamicin-exposed groups in Experiment 2.

RESULTS

The presentation of results will focus on NDF bandwidth and NDF peak location as the two primary dependent measures of neural firing density across stimulus types in Experiment 1 and across normal-hearing and gentamicin-exposed groups in Experiment 2. However, data for unmasked CAP amplitudes are presented at the outset to demonstrate the effectiveness of chirps as stimuli for evoking CAPs. N_1 latency data for both experiments were not analyzed in depth for this study but are shown in Figures D.1 and D.2 of Appendix D.

Unmasked CAP Amplitudes

Representative CAPs evoked in normal-hearing gerbils with 2 kHz tonebursts and chirps at 60 dB pSPL are shown in the top panel of Figure 5. In addition to being nearly 10 times larger in magnitude than the 2 kHz toneburst CAP (Fig. 5, top left panel), the chirp CAP (Fig. 5, top right panel) has narrower N_1 morphology. Comparing the unmasked N_1 amplitudes across stimulus type and stimulus level (Fig. 5,

bottom panel) indicates that chirps at 60 dB pSPL produced the largest CAPs and 2 kHz tonebursts at 60 dB pSPL produced the smallest CAPs. Interestingly, chirps at 30 dB pSPL generated larger CAPs than 2 kHz tonebursts at 90 dB pSPL. Calculating the coefficients of variation (CV, standard deviation/mean) of the unmasked amplitude data revealed that the amplitude measures for chirps at 60 dB pSPL were the least variable (CV = 0.16) and the amplitude measures for 2 kHz tonebursts at 90 dB pSPL were the most variable (CV = 0.32) across animals. The CVs of the other stimulus conditions were 0.24, 0.24, and 0.27, for 2 kHz tonebursts at 60 dB pSPL, chirps at 90 dB pSPL, and chirps at 30 dB pSPL, respectively.

To determine the variability of the unmasked amplitude measures within animals, which served as the reference for normalization of the masked amplitude values, the within-animal CVs of the unmasked amplitudes were also calculated for the four stimulus conditions of Experiment 1 and the two stimulus conditions of Experiment 2. The highest within-animal CV of 0.22 was observed for the unmasked amplitudes of CAPs to chirps at 90 dB pSPL from a normal-hearing gerbil. The lowest within-animal CV of 0.01 was noted for the unmasked amplitudes of CAPs to chirps at 60 dB pSPL, also from a normal-hearing gerbil. The mean within-animal CV for unmasked amplitude across stimulus conditions for the normal-hearing group were 0.11, 0.04, 0.06, and 0.08, for CAPs to chirps at 90 dB pSPL, chirps at 60 dB pSPL, 2 kHz tonebursts at 90 dB pSPL, and 2 kHz tonebursts at 60 dB pSPL, respectively. For the gentamicin-exposed group, the mean within-animal CV for unmasked amplitudes was 0.11 for chirps at 90 dB pSPL and 0.10 for chirps at 60 dB pSPL.

Experiment 1: Cumulative Amplitude Functions (CAFs)

Figure 6 shows the normalized N_1 amplitude growth data (thin lines) for the nine normal-hearing gerbils in Experiment 1 with the mean of their respective CAFs (thick lines) for chirps and 2 kHz tonebursts at 90 dB pSPL and 60 dB pSPL. The variance of the data across animals and across conditions was largest for 2 kHz tonebursts at 60 dB pSPL and smallest for chirps at 60 dB pSPL. The mean CAF for chirps at 90 dB pSPL grows gradually and just begins to saturate near the base (i.e., 11 mm from apex). In contrast, the mean CAF for 2 kHz tonebursts at 90 dB pSPL rises quickly and saturates by

approximately 9 mm from the apex. The CAF for chirps at 60 dB pSPL is similar to the pattern observed for 2 kHz tonebursts at 90 dB pSPL whereas the CAF for 2 kHz tonebursts at 60 dB pSPL begins to grow close to the apex and saturates approximately 7 mm from the apex. The N_1 amplitude function depicted with the dashed thin line in the upper right panel (2 kHz toneburst – 90 dB pSPL) was determined to be an outlier and was excluded from statistical analysis because its initial masked amplitude was more than two standard deviations (SD) above the mean of the initial masked amplitude across all amplitude functions in Experiment 1. The mean coefficients of determination (R^2) indicate that the four-parameter sigmoid function accounts for a large majority of the variance in the N_1 amplitude data for all four stimulus conditions. The assumptions of normality and constant variance were satisfied for all CAFs for all four stimulus conditions with one exception: the assumption of constant variance was violated for one CAF for chirps at 90 dB pSPL.

Experiment 1: Neural Density Functions (NDFs)

Figure 7 displays individual NDFs (thin lines) with their corresponding mean NDFs (heavy lines) for each of the four stimulus conditions. The NDFs illustrate, as did the CDFs, that the variance across animals was largest for 2 kHz tonebursts at 60 dB pSPL and smallest for chirps at 60 dB pSPL. The individual NDF shown with the dashed line in the upper right panel (2 kHz toneburst – 90 dB pSPL) represents the outlier that was described previously in Figure 6.

Figure 8 illustrates the differences in mean NDF bandwidth and mean NDF peak location for chirps (solid lines) and 2 kHz tonebursts (dashed lines) at 90 and 60 dB pSPL. At 90 dB pSPL (Fig. 8, left panel), the mean NDF for chirps was significantly broader ($p = 0.04$) and peaked significantly closer to the base ($p = 0.001$) than the mean NDF for 2 kHz tonebursts. At 60 dB pSPL (Fig. 8, right panel), the mean NDF for 2 kHz tonebursts was significantly broader than the mean NDF for chirps ($p = 0.04$) although the mean NDF for chirps peaked significantly closer to the base ($p < 0.001$). Table 1 summarizes the descriptive statistics and the results of the paired samples t-tests used to compare the mean of the paired differences for the two variables across stimulus type at both levels. The assumption

of normality was satisfied by the values for NDF bandwidth and NDF peak location for all four stimulus conditions in Experiment 1 per Shapiro-Wilk's test of normality.

Experiment 2: Gentamicin-Induced Changes in CM Amplitude and CAP Threshold

The left panel of Figure 9 illustrates that the amplitude of the CM, evoked with 16 kHz tones at 80 dB pSPL, decreased exponentially over a course of minutes following application of 200 µg of gentamicin to the round window niche. Dose-response curves for gentamicin doses of 50 and 100 µg are shown for comparison. All 10 of the animals included in Experiment 2 experienced at least a 50% reduction in CM amplitude after an exposure to 200 µg of gentamicin lasting at least 15 minutes.

The right panel of Figure 9 shows post-gentamicin shifts in CAP thresholds for chirps (measured after removal of gentamicin from the niche) and toneburst stimuli (measured after completion of post-gentamicin masked CAP conditions). Shifts in chirp CAP thresholds ranged from 10 to 25 dB while shifts in toneburst CAP thresholds generally increased as stimulus frequency increased. Comparing the post-gentamicin measures of chirp CAP threshold to the measures of chirp CAP threshold at the completion of the post-gentamicin masked CAP conditions revealed that the largest within-animal fluctuation was 10 dB and the group mean fluctuation was less than 5 dB, indicating that threshold shifts were generally stable after exposure to gentamicin and multiple presentations of masking noise.

However, progressive elevations in CAP thresholds and steady decline in unmasked CAP amplitudes following gentamicin exposure were observed in two animal experiments that began with chirps at 90 dB pSPL. Both experiments were terminated prematurely and a synergistic effect of gentamicin plus noise exposure (see Literature Review in Appendix A) was suspected due to the high levels of noise that were required to achieve the initial 80% reduction in amplitude of the high-level CAPs. Progressive CAP threshold elevation and declining CAP amplitude were observed in one other animal experiment that started with CAPs to chirps at 60 dB pSPL and consequently lower levels of masking noise.

Experiment 2: CAF & NDF Comparisons across Groups

The top panels of Figure 10 compare the individual data and mean CAFs for chirps of the post-gentamicin group to normal ranges constructed with the data from Experiment 1. At 90 dB pSPL, the individual N_1 amplitude functions of the 10 gentamicin-exposed gerbils (top left panel, thin lines) fell essentially within the normal range (mean of N_1 amplitude +/- 2SD; gray area). In contrast, at 60 dB pSPL a large portion of the functions for 6 out of the 10 gentamicin-exposed animals (top right panel, thin lines) fell outside the normal range. The mean post-gentamicin CAF at 60 dB pSPL (thick dashed line, top right panel) grows at a similar rate as the normal range; however, the post-gentamicin CAF is shifted nearly 1 mm closer to the apex than the normal range. The mean R^2 values for the CAF fits of the post-gentamicin data (0.93 for chirps at 90 dB pSPL and 0.96 for chirps at 60 dB pSPL, respectively) suggest that the sigmoid function accounts for a large majority of the variance in the N_1 amplitude data for both stimulus conditions. The assumptions of normality and constant variance were satisfied for all CAFs for both stimulus conditions with two exceptions: the assumption of constant variance was violated for two CAFs for chirps at 60 dB pSPL.

The bottom panels of Figure 10 compare the individual and mean post-gentamicin NDFs to the normal NDF ranges (mean +/- 2SD; gray areas) established with the data from Experiment 1. Similar to the N_1 amplitude plots in the upper panels, the NDFs of the two groups essentially overlap for chirps at 90 dB pSPL (bottom left panel), whereas for chirps at 60 dB pSPL (bottom right panel), the distributions of the two groups appear to differ. Table 2 summarizes the descriptive statistics and results of the independent samples t-tests (SPSS 17.0) of the difference across groups for mean bandwidth and mean peak location. As hypothesized, there was not a significant difference between groups for mean NDF bandwidth or mean NDF peak location for chirps at 90 dB pSPL. For chirps at 60 dB pSPL, mean NDF bandwidth was not significantly different across groups; however, the mean NDF peak location for the gentamicin-exposed group was significantly closer ($p = 0.01$) to the apex than the mean NDF peak location for the normal-hearing group (open circle). As noted in Table 2 and illustrated in Figure 10, the

assumption of equal variance was violated for the NDF peak location data for chirps at 60 dB pSPL. The assumption of equal variance was satisfied for the NDF bandwidth data for chirps at 60 dB pSPL and for the NDF bandwidth and peak location data for chirps at 90 dB pSPL. The assumption of normality was satisfied for the NDF bandwidth and NDF peak location data for both chirp conditions of both groups (i.e., normal and post-gentamicin) according to the Shapiro-Wilk test of normality (SPSS 17.0).

Experiment 2: Variability in NDF Peak Location

To determine the possible contributors to the large variability observed in the NDF peak location for chirps at 60 dB pSPL, several scatter plots were constructed and correlation analyses were performed. Figure 11 illustrates a significant negative correlation (r = -0.74; p = 0.003) between the post-gentamicin shift in NDF peak location for chirps at 60 dB pSPL and the post-gentamicin shift in chirp CAP thresholds. The shift in NDF peak location was determined by calculating the differences between the individual post-gentamicin peak locations and the mean NDF peak location of the normal-hearing group for chirps at 60 dB pSPL. The individual shifts in chirp CAP threshold were determined by calculating the difference between the pre-exposure threshold and the post-exposure threshold (measured immediately following the 15-minute gentamicin-exposure period). Filled circles (n = 10) represent the animals that met the inclusion criteria for Experiment 2. Open circles (n = 4) represent animals that were excluded from analysis due to progressive CAP threshold shifts during the course of data collection (two upper circles) or due to minimal chirp CAP threshold shifts or insufficient reduction in CM amplitude following gentamicin application (two lower circles). Other scatter plots between the shift in NDF peak location for chirps at 60 dB pSPL and other post-gentamicin measures including toneburst CAP threshold shift and CM amplitude reduction did not reveal any significant correlations.

DISCUSSION

The motives for this study were to determine if high-level chirps trigger a broader spread of synchronous neural firing along the cochlear partition than high-level low frequency tonebursts and to

determine if high-level NDFs are unaltered by OHC pathology. The results support both central hypotheses and provide additional data suggesting that NDFs constructed with chirps at a moderate level (i.e., 60 dB pSPL) are influenced by OHC pathology. Other observations relating to chirp CAP amplitude, CAP latency shifts, the design of the chirp stimulus, the high-pass masking paradigm, and the data-fitting procedure have implications for future research and clinical application.

Experiment 1: NDF Differences across Stimulus Type

The results of Experiment 1 showing broader NDF bandwidths for high-level chirps than for high-level low frequency tonebursts support the hypothesis that high-level chirps evoke a broader spread of synchronous neural firing along the cochlear partition than high-level low frequency (2 kHz) tonebursts. On average, the NDF bandwidths for chirps at 90 dB pSPL were 1.5 times broader and peaked nearly 2 mm closer to the base of the cochlea than those for 2 kHz tonebursts at 90 dB pSPL (Fig. 8, left panel). The NDF bandwidth comparison across stimulus type for the moderate level of 60 dB pSPL (Fig. 8, right panel) suggests that moderate-level 2 kHz tonebursts evoke a larger spread of synchronous neural firing than moderate-level chirps. However, as displayed in the bottom right panel of Figure 7, NDF bandwidth for 2 kHz tonebursts at 60 dB pSPL was highly variable. The NDF peak location for 2 kHz tonebursts at 60 dB pSPL was also considerably more variable than for chirps at 60 dB pSPL, but the mean data suggest that the distribution of neural firing evoked by moderate-level chirps peaks significantly closer to the base than for moderate-level low frequency tonebursts.

Experiment 2: NDF Comparisons across Groups

The negligible differences between high-level NDFs for the normal-hearing and gentamicin-exposed groups (Fig. 10, bottom left panel) support the hypothesis that gentamicin-induced OHC pathology does not significantly alter the spread of neural firing evoked with high-level stimuli. The secondary observation that gentamicin-induced OHC pathology did significantly alter the peak location of NDFs constructed with chirps at a moderate level (i.e., 60 dB pSPL; Fig. 10, bottom right panel) is consistent with previous research (e.g., Dallos and Harris, 1978; Ruggero and Rich,1991; Fridberger et

al., 2002) suggesting OHCs act primarily to enhance basilar membrane displacement for low to moderate-level inputs.

Despite receiving the same 200 µg dose of gentamicin, the peak location of post-gentamicin NDFs for chirps at 60 dB pSPL (Fig. 10, bottom right panel) varied by as much as 2 mm. This observation suggests inter-animal differences in gentamicin susceptibility that are consistent with the results of Wanamaker et al. (1998) indicating differing amounts of hair cell damage in gerbils receiving equivalent transtympanic doses of gentamicin. The significant negative correlation (r = -0.74; p = 0.003) between the shift in peak location for moderate-level NDFs and chirp CAP threshold shift (Fig. 11) suggests that chirp CAP threshold shifts may provide an estimate of gentamicin-induced shifts in neural firing evoked with moderate-level stimuli.

Unmasked CAP Amplitudes

The chirp CAP waveforms displayed in Figure 5 and in Appendix C were considerably larger in amplitude and had narrower N_1 morphology than 2 kHz toneburst CAPs. These observations suggest that chirps generate synchronous neural firing across a larger number of auditory neurons than 2 kHz tonebursts. Figure 5 also illustrates that, on average, chirps at 90 dB pSPL yield smaller CAP amplitudes than chirps at 60 dB pSPL. This finding may be related to the fact that the chirp used in this study was constructed with near-threshold CAP latency data and its instantaneous frequency was not adjusted to account for differences in the traveling wave velocity across different signal levels (Fobel and Dau, 2004). Dau et al. (2000) also held the instantaneous frequency of their chirp stimulus constant across level and observed a similar roll-off in wave-V amplitude of ABRs evoked with high-level chirps.

The across-animal coefficients of variation (CV) of the unmasked CAP amplitude were smaller for chirps (0.24 for 90 dB pSPL, 0.16 for 60 dB pSPL) than for 2 kHz tonebursts (0.32 for 90 dB pSPL, 0.24 for 60 dB pSPL) suggesting that chirp CAP amplitude is more stable across animals for a given stimulus level than 2 kHz toneburst CAP amplitude. The mean within-animal CV of unmasked CAP amplitude was larger for chirps at 90 dB pSPL (0.11) than for 2 kHz tonebursts at 90 dB pSPL (0.06)

suggesting that high-level chirp CAP amplitude is slightly less stable over a recording session in one animal than high-level toneburst CAP amplitude. The opposite was observed for the CV of the unmasked CAP amplitude for the two stimuli at 60 dB pSPL (chirps = 0.04; 2 kHz tonebursts = 0.08) suggesting that chirp CAP amplitude at that level is more stable during one recording session than 2 kHz toneburst CAP amplitude.

CAP Latency Shifts

As mentioned above in the Results section, N_1 latency data were not analyzed in depth for this study but are shown in Appendix D. Figure D.1 displays the data for the four stimulus conditions of Experiment 1 and Figure D.2 shows the data for the two stimulus conditions of Experiment 2. Both figures plot the shifts in N_1 peak latency (masked-unmasked latency) as a function high-pass noise cutoff frequency. The horizontal line at zero represents the baseline peak latency for unmasked CAPs. The latency shift functions are generally consistent with the theory suggested by Teas et al. (1962) and the data from others (e.g. Elberling, 1974, Don et al., 1979, Evans and Elberling, 1982) that the location of synchronous neural firing for moderate and high-level stimuli is "pushed" toward the apex proportional to the high-pass cutoff frequency of masking noise. The trends in latency shift resemble the inverse of the patterns observed for N_1 amplitude growth. The latency functions for the gentamicin-exposed group in Experiment 2 (Fig. D.2) show smaller shifts in latency and more variability when compared to the trends of the chirp CAP latency functions of the normal-hearing group.

Chirp Stimulus

As mentioned above, the instantaneous frequency, and therefore the duration, of the chirp stimulus used in this study was held constant for both stimulus levels (i.e., 60 and 90 dB pSPL). In addition to being smaller in amplitude than chirp CAPs at 60 dB pSPL, chirp CAPs at 90 dB pSPL (e.g. Fig. 3, left panel; Fig. C.1) also had broader N_1 morphology than responses at 60 dB pSPL (Fig. 5, top right panel; Fig. C.2). Generating level-specific chirps may further optimize neural synchrony and increase amplitudes of high-level chirp CAPs.

Considering the entire span of the mean high-level NDF for chirps (Fig. 8, right panel), the chirp stimulus was effective in triggering neural firing across 8.5 mm (3 to 11.5 mm from the apex) of the cochlear partition. However, the apparent lack of apical neural firing before the 3 mm location suggests that dropping the low-frequency edge of the chirp spectrum from 1 kHz to 250 or 500 Hz and/or increasing the spectral magnitude of the low frequency energy of the chirp may further extend neural firing towards the apex. Extending the high-frequency edge of the chirp spectrum past 60 kHz and adding 2-3 masker cutoff frequencies above 45 kHz may also improve identification of the saturation point of N_1 amplitude growth functions for high-level chirps (e.g. Fig. 6, top left panel).

High-Pass Noise Masking Paradigm

Similar to the high-pass noise masking paradigms used in previous studies (e.g., Teas et al., 1962; Shore and Nuttall, 1985; see Literature Review in Appendix A), the masking paradigm in this study led to decreases in N_1 amplitude and increases in N_1 latency with decreases in the high-pass noise cutoff frequency (e.g. Fig. 3, right panel). However, the masking paradigms of previous studies have generally included 6-8 high-pass cutoff frequencies representing octave intervals (e.g. Teas et al., 1962; Don et al., 2005) with one exception: the study in guinea pig by Shore and Nuttall (1985) used 18 cutoff frequencies representing 1/3 octave increments between 0.4 and 20 kHz. The masking paradigm of the current study included 25 cutoff frequencies representing 0.25 mm increments along the first 3 mm of the basal turn and 0.5 mm increments for the middle through apical regions of the gerbil cochlea (3-11 mm) to provide distance-based amplitude growth functions with relatively high resolution. The technique of deriving neural density functions from cumulative amplitude (sigmoid) functions describing the N_1 amplitude growth data is novel. Previous studies have primarily focused on calculating derived band waveforms to infer regional cochlear contributions to the CAP as well as predicting behavioral hearing thresholds (see Literature Review in Appendix A).

Sigmoid Model Performance

The mean (R^2) values for the CAF fits of both experiments suggest that the four-parameter sigmoid function accounts for a large majority of the variance in the N_1 amplitude data for all stimulus conditions. For Experiment 1 (Fig. 6), the sigmoid function achieved the best fit for the amplitude data for chirps at 60 dB pSPL with a mean R^2 of 0.99 (range = 0.985-0.998). The lowest mean R^2 of 0.92 (range = 0.796-0.976) was observed for the fits of the amplitude data for chirps at 90 dB pSPL. The lower values and larger range for the R^2 values for the fits of the data for chirps at 90 dB pSPL is not unexpected given the lack of a definite point of saturation for the majority of the amplitude growth functions. Accordingly, the parameter *a*, which scales the inflection point of N_1 amplitude growth, had to be manually constrained for 7 of the 9 fits of the amplitude data for chirps at 90 dB pSPL. Without manual constraints, the parameter *a* was not significant and the fitted function tended towards exponential growth. For each of the other three stimulus conditions, the parameter *a* only had to be manually constrained for 1 of the 9 fits. The parameter *b*, that governs the rate of growth of the CAF, also required manual constraints to be retained as a significant parameter and/or to preserve constant variance in 3 of the 9 fits of the data for chirps at 90 dB pSPL and 1 of the 9 fits of the data for 2 kHz tonebursts at 60 dB pSPL. For Experiment 2 (Fig. 10, top panels), the R^2 values for the post-gentamicin CAFs for chirps at 90 dB pSPL ranged from 0.89 to 0.97. Similar to the CAF fits of the normal data for chirps at 90 dB pSPL, the sigmoid parameter *a* had to be manually constrained for the majority of animals (9 out of 10) to achieve significance for all parameters. The R^2 values for the post-gentamicin CAFs for chirps at 60 dB pSPL ranged from 0.92 to 0.98 and no manual constraints of the sigmoid parameters were necessary. Objectivity in choosing manual constraints was maintained by focusing on the goal of maximizing the R^2 value while retaining significance for all four parameters.

Alternative Method of Analysis

Taking the analytical derivative of the four-parameter sigmoid function (Eq. 2) used to fit the N_1 amplitude growth data dictates NDFs with one peak and a smooth distribution (Fig. 8 and Fig. 10).

However, the subtle fluctuations in the normalized N_1 amplitude data may provide valuable information for differential diagnosis. An alternative analysis method that would preserve the "fine-structure" of neural firing involves bypassing the sigmoid fits and plotting the numerical derivative of the normalized N_1 amplitude data (e.g., Fig. E.1, Appendix E). Comparing the numerical NDFs (Fig. E.1) to the corresponding analytical NDFs (Fig. 8 and Fig. 10, bottom panels) reveals that the NDFs for high-level chirps differ considerably between the two approaches. For example, the mean analytical NDF for chirps at 90 dB pSPL in Experiment 1 (Fig. 8, left panel) suggests that neural firing density accumulates gradually beginning at approximately 3 mm from the apex whereas the mean numerical NDF for the same data captures a bump in neural firing density between 1 and 4 mm from the apex. The most prominent peak of the three-peaked numerical NDF for chirps at 90 dB pSPL occurs at approximately 10 mm from the apex suggesting that peak firing density is nearly 2 mm closer to the base than suggested by the analytical NDF (8.22 mm from apex). Constructing NDFs in this manner also avoids the dilemma of choosing manual constraints for sigmoid fits of quasi-sigmoid data (e.g., amplitude functions for chirps at 90 dB pSPL).

Future Directions

Building on the outcomes of this study, the next experiment will be launched to determine if high-level neural density functions are correlated with the distribution of surviving auditory neurons in animals with partial lesions of the auditory nerve. If CAP-derived NDFs can reliably predict the extent and location of neural pathology, a similar masking paradigm could then be implemented in electrocochleography recording protocols for human patients. Automation of the masker presentations and corresponding CAP recordings would allow extra time for repeat sweeps through the entire masking protocol. Automation would also aid in quickly constructing NDFs for chirps across a range of signal levels (e.g., near threshold to high levels) in normal and impaired ears. Additional examinations of the data collected for this study to assess the fine-structure of individual numerical NDFs, to plot derived-band waveforms, and to analyze masked latency shifts may also provide valuable information.

CONCLUSIONS

1. Chirp stimuli evoke large CAPs with clear morphology and minimal signal averaging making them advantageous for use in clinical situations where test time may be limited.
2. High-level chirps trigger a broader spread of synchronous neural firing along the cochlear partition than high-level low frequency (2 kHz) tonebursts indicating that chirps are superior stimuli for mapping auditory nerve density across the majority of the cochlea with a high-pass masking paradigm.
3. Gentamicin-induced OHC pathology does not significantly alter the distribution of neural firing evoked by high-level chirps pointing to their utility in providing reliable maps of auditory nerve density in impaired ears.

REFERENCES

Agterberg, M. J., Versnel, H., van Dijk, L. M., de Groot, J. C. & Klis, S. F. (2009) Enhanced survival of spiral ganglion cells after cessation of treatment with brain-derived neurotrophic factor in deafened guinea pigs. *J Assoc Res Otolaryngol,* 10, 355-67.

Al-momani, M. O., Ferraro, J. A., Gajewski, B. J. & Ator, G. (2009) Improved sensitivity of electrocochleography in the diagnosis of Meniere's disease. *Int J Audiol,* 48, 811-9.

Bentler, R. & Chiou, L. K. (2006) Digital noise reduction: an overview. *Trends Amplif,* 10, 67-82.

Bentler, R., Wu, Y. H., Kettel, J. & Hurtig, R. (2008) Digital noise reduction: outcomes from laboratory and field studies. *Int J Audiol,* 47, 447-60.

Bhatt, K. A., Liberman, M. C. & Nadol, J. B., Jr. (2001) Morphometric analysis of age-related changes in the human basilar membrane. *Ann Otol Rhinol Laryngol,* 110, 1147-53.

Bierer, J. A. & Faulkner, K. F. (2010) Identifying cochlear implant channels with poor electrode-neuron interface: partial tripolar, single-channel thresholds and psychophysical tuning curves. *Ear Hear,* 31, 247-58.

Blanchet, C., Eróstegui, C., Sugasawa, M., & Dulon, D. (2000) Gentamicin blocks ACh-evoked K^+ current in guinea-pig outer hair cells by impairing Ca^{2+} entry at the cholinergic receptor. *J Physiol*, 525.3, 641-654.

Bone, R. C., Crowley, D. & Rauchbach, E. (1972) 8th nerve round window action potentials masked by high frequency noise in rats and guinea pigs: a comparative study. *Laryngoscope,* 82, 1499-513.

Bredberg, G. (1968) *Cellular pattern and nerve supply of the human organ of Corti,* (Trans. exp. [Almqvist & Wiksell], Uppsala,.

Briaire, J. J. & Frijns, J. H. (2006) The consequences of neural degeneration regarding optimal cochlear implant position in scala tympani: a model approach. *Hear Res,* 214, 17-27.

Brown, J.J., Brummett, R.E., Meikle, M.B., & Vernon, J. (1978) Combined effects of noise and neomycin. *Acta Otolaryngol*, 86, 394-400.

Chertoff, M. E. (2004) Analytic treatment of the compound action potential: estimating the summed post-stimulus time histogram and unit response. *J Acoust Soc Am,* 116, 3022-30.

Chertoff, M. E., Lichtenhan, J. T., Tourtillott, B. M. & Esau, K. S. (2008) The influence of noise exposure on the parameters of a convolution model of the compound action potential. *J Acoust Soc Am,* 124, 2174-85.

Chertoff, M.E., Lichtenhan, J.T., & Willis, M. (2010) Click- and chirp-evoked human compound action potentials. *J Acoust Soc Am,* 127, 2992-2996.

Chung, K., Zeng, F. G. & Acker, K. N. (2006) Effects of directional microphone and adaptive multichannel noise reduction algorithm on cochlear implant performance. UC Irvine.

Cone-Wesson, B., Vohr, B. R., Sininger, Y. S., Widen, J. E., Folsom, R. C., Gorga, M. P. & Norton, S. J. (2000) Identification of neonatal hearing impairment: infants with hearing loss. *Ear Hear,* 21, 488-507.

Crowe, S. J., Guild, S. R. & Polvogt, L. M. (1934) Observations on the pathology of high-tone deafness. *Bull Johns Hopkins Hosp,* 54, 315-379.

Crowley, D. E., Swain, R. E., Schramm, V. L. & Swanson, S. N. (1972) Analysis of age-related changes in electric responses from the inner ear of rats. *Ann Otol Rhinol Laryngol,* 81, 739-46.

Cunningham, M. & Cox, E. O. (2003) Hearing assessment in infants and children: recommendations beyond neonatal screening. *Pediatrics,* 111, 436-40.

Dallos, P., Billone, M. C., Durrant, J. D., Wang, C. & Raynor, S. (1972) Cochlear inner and outer hair cells: functional differences. *Science,* 177, 356-8.

Dallos, P. & Harris, D. (1978) Properties of auditory nerve responses in absence of outer hair cells. *J Neurophysiol,* 41, 365-83.

Dau, T., Wegner, O., Mellert, V. & Kollmeier, B. (2000) Auditory brainstem responses with optimized chirp signals compensating basilar-membrane dispersion. *J Acoust Soc Am,* 107, 1530-40.

de Boer, E. (1980) Auditory physics: Physical principles in hearing theory I. *Phys Rep,* 62, 87-174.

Dolan, D. F., Teas, D. C. & Walton, J. P. (1983) Relation between discharges in auditory nerve fibers and the whole-nerve response shown by forward masking: an empirical model for the AP. *J Acoust Soc Am,* 73, 580-91.

Don, M. & Eggermont, J. J. (1978) Analysis of the click-evoked brainstem potentials in man using high-pass noise masking. *J Acoust Soc Am,* 63, 1084-92.

Don, M., Eggermont, J. J. & Brackmann, D. E. (1979) Reconstruction of the audiogram using brain stem responses and high-pass noise masking. *Ann Otol Rhinol Laryngol Suppl,* 57, 1-20.

Don, M., Elberling, C. & Maloff, E. (2009) Input and output compensation for the cochlear traveling wave delay in wide-band ABR recordings: Implications for small acoustic tumor detection. *J Am Acad Audiol,* 20, 99-108.

Don, M., Kwong, B., Tanaka, C., Brackmann, D. & Nelson, R. (2005) The stacked ABR: a sensitive and specific screening tool for detecting small acoustic tumors. *Audiol Neurootol,* 10, 274-90.

Don, M., Masuda, A., Nelson, R. & Brackmann, D. (1997) Successful detection of small acoustic tumors using the stacked derived-band auditory brain stem response amplitude. *Am J Otol,* 18, 608-21; discussion 682-5.

Earl, B. R. & Chertoff, M. E. (2010) Predicting auditory nerve survival using the compound action potential. *Ear Hear,* 31, 7-21.

Edge, A. S. & Chen, Z. Y. (2008) Hair cell regeneration. *Curr Opin Neurobiol,* 18, 377-82.

Eggermont, J. J. (1976) Analysis of compound action potential responses to tone bursts in the human and guinea pig cochlea. *J Acoust Soc Am,* 60, 1132-9.

Eggermont, J. J. (1977) Compound actionpotential tuning curves in normal and pathological human ears. *J Acoust Soc Am,* 62, 1247-51.

Elberling, C. (1974) Action potentials along the cochlear partition recorded from the ear canal in man. *Scand Audiol,* 3, 13-19.

Elberling, C. & Don, M. (2008) Auditory brainstem responses to a chirp stimulus designed from derived-band latencies in normal-hearing subjects. *J Acoust Soc Am,* 124, 3022-37.

Elberling, C., Don, M., Cebulla, M. & Sturzebecher, E. (2007) Auditory steady-state responses to chirp stimuli based on cochlear traveling wave delay. *J Acoust Soc Am,* 122, 2772-85.

Evans, E. F. & Elberling, C. (1982) Location-specific components of the gross cochlear action potential: an assessment of the validity of the high-pass masking technique by cochlear nerve fibre recording in the cat. *Audiology,* 21, 204-27.

Felder, E. & Schrott-Fischer, A. (1995) Quantitative evaluation of myelinated nerve fibres and hair cells in cochleae of humans with age-related high-tone hearing loss. *Hear Res,* 91, 19-32.

Feller, W. (1968) *An Introduction to Probability Theory and Its Applications,* (Trans.) John Wiley & Sons, Inc., New York.

Ferraro, J. A. & Durrant, J. D. (2006) Electrocochleography in the evaluation of patients with Meniere's disease/endolymphatic hydrops. *J Am Acad Audiol,* 17, 45-68.

Firszt, J. B., Holden, L. K., Reeder, R. M. & Skinner, M. W. (2009) Speech recognition in cochlear implant recipients: comparison of standard HiRes and HiRes 120 sound processing. *Otol Neurotol,* 30, 146-52.

Fobel, O. & Dau, T. (2004) Searching for the optimal stimulus eliciting auditory brainstem responses in humans. *J Acoust Soc Am,* 116, 2213-22.

Forge, A. & Schacht, J. (2000) Aminoglycoside antibiotics. *Audiol Neurootol,* 5, 3-22.

Fridberger, A., Zheng, J., Parthasarathi, A., Ren, T. & Nuttall, A. (2002) Loud sound-induced changes in cochlear mechanics. *J Neurophysiol,* 88, 2341-8.

Gibson, W. P. & Sanli, H. (2007) Auditory neuropathy: an update. *Ear Hear,* 28, 102S-106S.

Goldstein, M. H. J. & Kiang, N. Y. S. (1958) Synchrony of neural activity in electric responses evoked by transient acoustic stimuli. *J Acoust Soc Am,* 30, 107-114.

Greenwood, D. D. (1990) A cochlear frequency-position function for several species-29 years later. *J Acoust Soc Am,* 87, 2592-605.

Guild, S. R., Bunch, C. C. & Polvogt, L. M. (1931) Correlations of differences in the density of innervation of the organ of Corti with differences in the acuity of hearing, including evidence as to the location in the human cochlea of the receptors for certain tones. *Acta Otolaryngol,* 15, 269-308.

Hall, R. D. (1990) Estimation of surviving spiral ganglion cells in the deaf rat using the electrically evoked auditory brainstem response. *Hear Res,* 45, 123-36.

Heydt, J. L., Cunningham, L. L., Rubel, E. W. & Coltrera, M. D. (2004) Round window gentamicin application: an inner ear hair cell damage protocol for the mouse. *Hear Res,* 192, 65-74.

Husmann, K. R., Morgan, A. S., Girod, D. A. & Durham, D. (1998) Round window administration of gentamicin: a new method for the study of ototoxicity of cochlear hair cells. *Hear Res,* 125, 109-19.

Koch, D. B., Osberger, M. J., Segel, P. & Kessler, D. (2004) HiResolution and conventional sound processing in the HiResolution bionic ear: using appropriate outcome measures to assess speech recognition ability. *Audiol Neurootol,* 9, 214-23.

Kroese, A. B., Das, A. & Hudspeth, A. J. (1989) Blockage of the transduction channels of hair cells in the bullfrog's sacculus by aminoglycoside antibiotics. *Hear Res,* 37, 203-17.

Li, H. & Steyger, P. S. (2009) Synergistic ototoxicity due to noise exposure and aminoglycoside antibiotics. *Noise Health,* 11, 26-32.

Lichtenhan, J. T. & Chertoff, M. E. (2008) Temporary hearing loss influences post-stimulus time histogram and single neuron action potential estimates from human compound action potentials. *J Acoust Soc Am,* 123, 2200-12.

Matsuoka, A. J., Kondo, T., Miyamoto, R. T. & Hashino, E. (2007) Enhanced survival of bone-marrow-derived pluripotent stem cells in an animal model of auditory neuropathy. *Laryngoscope,* 117, 1629-35.

Moeller, M. P. (2000) Early intervention and language development in children who are deaf and hard of hearing. *Pediatrics,* 106, E43.

Monzani, D., Galeazzi, G. M., Genovese, E., Marrara, A. & Martini, A. (2008) Psychological profile and social behaviour of working adults with mild or moderate hearing loss. *Acta Otorhinolaryngol Ital,* 28, 61-6.

Müller, M. (1996) The cochlear place-frequency map of the adult and developing Mongolian gerbil. *Hear Res,* 94, 148-56.

Neely, S. T., Norton, S. J., Gorga, M. P. & Jesteadt, W. (1988) Latency of auditory brain-stem responses and otoacoustic emissions using tone-burst stimuli. *J Acoust Soc Am,* 83, 652-6.

Neff, W. D. (1947) The effects of partial section of the auditory nerve. *Jour Comp and Physiol Psych,* 40, 203-215.

Nelson, E. G. & Hinojosa, R. (2003) Presbycusis: a human temporal bone study of individuals with flat audiometric patterns of hearing loss using a new method to quantify stria vascularis volume. *Laryngoscope,* 113, 1672-86.

Nelson, E. G. & Hinojosa, R. (2006) Presbycusis: a human temporal bone study of individuals with downward sloping audiometric patterns of hearing loss and review of the literature. *Laryngoscope,* 116, 1-12.

Ohlemiller, K. K. (2004) Age-related hearing loss: the status of Schuknecht's typology. *Curr Opin Otolaryngol Head Neck Surg,* 12, 439-43.

Ou, H., Dunn, C. C., Bentler, R. A. & Zhang, X. (2008) Measuring cochlear implant satisfaction in postlingually deafened adults with the SADL inventory. *J Am Acad Audiol,* 19, 721-34.

Parker, D. J. & Thornton, A. R. (1978) Cochlear travelling wave velocities calculated from the derived components of the cochlear nerve and brainstem evoked responses of the human auditory system. *Scand Audiol,* 7, 67-70.

Parker, D. J. & Thornton, A. R. (1978) Frequency specific components of the cochlear nerve and brainstem evoked responses of the human auditory system. *Scand Audiol,* 7, 53-60.

Parker, D. J. & Thornton, A. R. (1978) The validity of the derived cochlear nerve and brainstem evoked responses of the human auditory system. *Scand Audiol,* 7, 45-52.

Pauler, M., Schuknecht, H. F. & Thornton, A. R. (1986) Correlative studies of cochlear neuronal loss with speech discrimination and pure-tone thresholds. *Arch Otorhinolaryngol,* 243, 200-6.

Pauler, M., Schuknecht, H. F. & White, J. A. (1988) Atrophy of the stria vascularis as a cause of sensorineural hearing loss. *Laryngoscope,* 98, 754-9.

Picton, T. W., Ouellette, J., Hamel, G. & Smith, A. D. (1979) Brainstem evoked potentials to tonepips in notched noise. *J Otolaryngol,* 8, 289-314.

Poissant, S. F., Beaudoin, F., Huang, J., Brodsky, J. & Lee, D. J. (2008) Impact of cochlear implantation on speech understanding, depression, and loneliness in the elderly. *J Otolaryngol Head Neck Surg,* 37, 488-94.

Prijs, V. F. & Eggermont, J. J. (1981) Narrow-band analysis of compound action potentials for several stimulus conditions in the guinea pig. *Hear Res,* 4, 23-41.

Ruggero, M. A. & Rich, N. C. (1991) Furosemide alters organ of corti mechanics: evidence for feedback of outer hair cells upon the basilar membrane. *J Neurosci,* 11, 1057-67.

Schuknecht, H. F. (1955) Presbycusis. *Laryngoscope,* 65, 402-419.

Schuknecht, H. F. (1964) Further Observations on the Pathology of Presbycusis. *Arch Otolaryngol,* 80, 369-82.

Schuknecht, H. F. (1994) Auditory and cytocochlear correlates of inner ear disorders. *Otolaryngol Head Neck Surg,* 110, 530-8.

Schuknecht, H. F. & Gacek, M. R. (1993) Cochlear pathology in presbycusis. *Ann Otol Rhinol Laryngol,* 102, 1-16.

Schuknecht, H. F. & Woellner, R. C. (1953) Hearing losses following partial section of the cochlear nerve. *Laryngoscope,* 63, 441-65.

Sellick, P. M., Patuzzi, R. & Johnstone, B. M. (1982) Measurement of basilar membrane motion in the guinea pig using the Mossbauer technique. *J Acoust Soc Am,* 72, 131-41.

Sheppard, W. M., Wanamaker, H. H., Pack, A., Yamamoto, S. & Slepecky, N. (2004) Direct round window application of gentamicin with varying delivery vehicles: a comparison of ototoxicity. *Otolaryngol Head Neck Surg,* 131, 890-6.

Shore, S. E. & Nuttall, A. L. (1985) High-synchrony cochlear compound action potentials evoked by rising frequency-swept tone bursts. *J Acoust Soc Am,* 78, 1286-95.

Spoendlin, H. (1975) Retrograde degeneration of the cochlear nerve. *Acta Otolaryngol,* 79, 266-75.

Spoendlin, H. (1984) Factors inducing retrograde degeneration of the cochlear nerve. *Ann Otol Rhinol Laryngol,* 93, 76-82.

Spoor, A., Eggermont, J. J. & Odenthal, D. W. (1976) Comparison of human and animal data concerning adaptation and masking of eight nerve compound action potential. In: *Electrocochleography* (eds R. J. Ruben, C. Elberling & G. Salomon). pp. 183-198. University Park Press, Baltimore.

Stapells, D. R., Gravel, J. S. & Martin, B. A. (1995) Thresholds for auditory brain stem responses to tones in notched noise from infants and young children with normal hearing or sensorineural hearing loss. *Ear Hear,* 16, 361-71.

Stapells, D. R. & Picton, T. W. (1981) Technical aspects of brainstem evoked potential audiometry using tones. *Ear Hear,* 2, 20-9.

Stapells, D. R., Picton, T. W., Durieux-Smith, A., Edwards, C. G. & Moran, L. M. (1990) Thresholds for short-latency auditory-evoked potentials to tones in notched noise in normal-hearing and hearing-impaired subjects. *Audiology,* 29, 262-74.

Suga, F. & Lindsay, J. R. (1976) Histopathological observations of presbycusis. *Ann Otol Rhinol Laryngol,* 85, 169-84.

Suryadevara, A. C., Wanamaker, H. H. & Pack, A. (2009) The effects of sound conditioning on gentamicin-induced vestibulocochlear toxicity in gerbils. *Laryngoscope,* 119, 1166-70.

Suzuka, Y. & Schuknecht, H. F. (1988) Retrograde cochlear neuronal degeneration in human subjects. *Acta Otolaryngol Suppl,* 450, 1-20.

Szymanski, M. D., Henry, K. R. & Buchting, F. O. (1994) Albino and pigmented gerbil auditory function: influence of genotype and gentamicin. *Audiology,* 33, 63-72.

Teagle, H. F., Roush, P. A., Woodard, J. S., Hatch, D. R., Zdanski, C. J., Buss, E. & Buchman, C. A. (2010) Cochlear implantation in children with auditory neuropathy spectrum disorder. *Ear Hear,* 31, 325-35.

Teas, D. C., Eldridge, D. H. & Davis, H. (1962) Cochlear responses to acoustic transients: An interpretation of whole-nerve action potentials. *J Acoust Soc Am,* 34, 1438-1459.

Wanamaker, H. H., Gruenwald, L., Damm, K. J., Ogata, Y. & Slepecky, N. (1998) Dose-related vestibular and cochlear effects of transtympanic gentamicin. *Am J Otol,* 19, 170-9.

Wegner, O. & Dau, T. (2002) Frequency specificity of chirp-evoked auditory brainstem responses. *J Acoust Soc Am,* 111, 1318-29.

Williams, S. E., Zenner, H. P. & Schacht, J. (1987) Three molecular steps of aminoglycoside ototoxicity demonstrated in outer hair cells. *Hear Res,* 30, 11-8.

Ylikoski, J., Wersall, J. & Bjorkroth, B. (1974) Degeneration of neural elements in the cochlea of the guinea-pig after damage to the organ of corti by ototoxic antibiotics. *Acta Otolaryngol Suppl,* 326, 23-41.

Yoshinaga-Itano, C., Sedey, A. L., Coulter, D. K. & Mehl, A. L. (1998) Language of early- and later-identified children with hearing loss. *Pediatrics,* 102, 1161-71.

Zerlin, S. & Naunton, R. F. (1976) Effects of high-pass masking on the whole-nerve response to third-octave audiometric clicks. In: *Electrocochleography* (eds R. J. Ruben, C. Elberling & G. Salomon). pp. 207-213. University Park Press, Baltimore.

Zwislocki, J. J. & Sokolich, W. G. (1973) Velocity and displacement responses in auditory-nerve fibers. *Science,* 182, 64-6.

Appendix A

Literature Review

Introduction

The development of diagnostic techniques to map auditory nerve survival may improve techniques for treating sensorineural hearing loss with hearing aids and cochlear implants and guide future implementation of regenerative therapies. This literature review focuses first on research related to the time course of auditory nerve degeneration secondary to organ of Corti damage and aging, and the capability of current clinic tools to diagnose auditory nerve degeneration. The focus will then shift to a review of several studies that have investigated the use of novel stimuli and masking paradigms to improve the performance of AEP measures for differential diagnosis of sensorineural hearing loss. Lastly, a summary is given of studies that have used gentamicin to induce OHC pathology in animal models and others that have investigated the effect of OHC pathology on CM and high-level CAP recordings.

Auditory Nerve Degeneration

Several studies of human temporal bones from elderly donors in the late 1800s and early 1900s (reviewed by Bredberg, 1968) found auditory nerve degeneration at the level of the osseous spiral lamina and the spiral ganglion cells (SGCs) to be the most common anatomical defect in the basal region of the cochlea. In these and later studies, concomitant atrophy of the organ of Corti was not always observed with auditory nerve degeneration (Bredberg, 1968; Spoendlin, 1975, 1984). When atrophy of the organ of Corti was observed, nerve degeneration was usually present but the extent of degeneration did not always correlate with the extent of loss of hair cells and supporting cells (Bredberg, 1968). Spoendlin (1975) observed that loss of IHCs and disruption of the blood supply to the cochleae of guinea pig and cat induced substantial retrograde degeneration in afferent auditory neurons. He also observed in other cochleae that OHC loss alone or supporting cell damage alone did not lead to significant nerve degeneration. Nerve degeneration without IHC loss was uncommon, but such observations suggested direct damage to dendrites of Type I afferents and/or other demyelinating conditions.

Spoendlin (1984) described two general categories of neural degeneration following axonal lesions; wallerian degeneration and secondary retrograde degeneration. Wallerian degeneration refers to atrophy of the axonal region that is separated from the neuronal cell body by a lesion. Secondary retrograde degeneration involves degeneration of the portion of the neuron containing the cell body. For type I afferent neurons that predominantly supply the IHCs of the cochlea, wallerian degeneration would refer to degeneration that begins at a dendritic lesion and progresses toward the synaptic connection with an IHC. Secondary retrograde degeneration of afferent auditory neurons progresses centrally from the axonal lesion toward the cell body in the spiral ganglion, eventually affecting the entire length of the neuron. Spoendlin (1984) states that wallerian degeneration has been observed to occur within hours in motor neurons while secondary retrograde degeneration in afferent neurons normally progresses over months and years.

Spoendlin's (1975) review of the data from guinea pig suggested that the process of retrograde degeneration in the auditory nerve following acoustic, mechanical, or ototoxic lesions to the cochlea begins with swelling of the peripheral dendrites and eventual rupture of the axonal membranes. Retrograde degeneration then progresses within days through the osseous spiral lamina to the level of the spiral ganglion. Subsequent degeneration and disappearance of SGCs occurs after several weeks with approximately 10% of SGCs surviving five months following cochlear lesions in guinea pig. Even one year post-lesion, 5-10% of the SGCs still appeared to be healthy. Other data cited by Spoendlin (1975) from congenitally deaf white cats suggested that 5-10% of SGCs remain viable over an eight year period. Significant numbers of surviving auditory neurons have also been observed in human temporal bones from donors with genetic conditions affecting the development and morphology of the organ of Corti (Spoendlin, 1975). In contrast, animal experiments involving disruption of the blood supply to the cochlea, found complete loss of viable auditory neurons (Spoendlin, 1975).

Other studies of human temporal bones aimed to find a relationship between the donors' audiometric records and the histological status of cochlear structures and auditory neurons. The early

work of Guild et al. (1931) documented atrophy of the organ of Corti and/or decreased innervation density in the basal region of the majority of cochleae from 15 patients with pre-mortem audiometric records showing elevated high frequency hearing thresholds. Crowe et al. (1934) also analyzed the temporal bones of 79 donors with moderate to severe high frequency hearing loss and found 75% of the cochleae to have basal atrophy of the organ of Corti and partial degeneration of the auditory nerve. The extent of nerve degeneration was observed to be greater in those ears with thresholds in the severe hearing loss range. These studies were followed by the extensive work of Schuknecht and colleagues (Schuknecht, 1955; Schuknecht, 1964; Otte et al., 1978; Suzuka and Schuknecht, 1988; Schuknecht and Gacek, 1993; Schuknecht, 1994) who suggested that the pathology contributing to presbycusis could be differentiated by audiometric shape. For example, Schuknecht and Gacek (1993) looked at serial sections of human temporal bones from 21 donors with audiometric records showing symmetric bilateral sensorineural hearing loss without any history of ear disorders or other risk factors for hearing loss. Their results suggested that a sharp drop in high frequency hearing thresholds resulted from atrophy of the organ of Corti and loss of hair cells and that unexpectedly poor word recognition ability was associated with degeneration and/or loss of auditory neurons. A uniform decline in hearing thresholds across frequency (i.e., flat audiometric pattern) was attributed to atrophy of the stria vascularis. Other patterns of presbycusis were thought to suggest a combination of several different cochlear and/or neural pathologies.

In contrast, findings of other temporal bone studies (e.g., Suga and Lindsay, 1976; Felder and Schrott-Fischer, 1995; Bhatt et al., 2001; Nelson and Hinojosa, 2003; Ohlemiller, 2004) have suggested that audiometric patterns of hearing loss could not consistently identify the location nor the extent of cochlear and neural pathology. For example, Nelson and Hinojosa (2003) analyzed the histological status of cochlear structures and auditory neurons of six patients with flat audiometric patterns of sensorineural hearing loss to test the idea that strial atrophy was responsible for this pattern. Their results indicated that only one of the six temporal bones examined had significant strial atrophy. Instead, all six cochleae had a statistically significant reduction in OHCs. Three of the six cochleae also showed a statistically

significant reduction in IHCs. Recent reviews by Mills (2006) and Nelson and Hinojosa (2006) also highlight data suggesting the limitations of behavioral audiometric tests for differential diagnosis of the underlying pathophysiology leading to sensorineural hearing loss and urge a test battery approach involving OAEs and AEPs.

In their 1953 study, Schuknecht and Woellner assessed both behavioral hearing thresholds and cortically evoked auditory potentials in six cats with partial lesions of the auditory nerve. Their results indicated that behavioral and electrophysiologic thresholds remained within the normal range with as much as an 80% loss of SGCs. However, when Schuknecht and Woellner (1953) measured the N_1 portion of the cortical response they observed that the maximum amplitude of N_1 decreased with increasing amounts of SGC degeneration. Hall (1990) induced varying degrees of spiral ganglion degeneration with neomycin in 16 rats and found strong positive correlations between the maximum amplitude of the first positive peak of electrically evoked ABR responses and the number of surviving ganglion cells. In a mouse model of noise exposure, Kujawa and Liberman (2008) also found that ABR amplitudes at high stimulus levels were better than thresholds in predicting auditory neuron degeneration. The strong positive correlations between maximum CAP amplitude and auditory nerve survival described by Earl and Chertoff (2010) are consistent with the findings of these previous studies and suggest that CAP amplitude may be a valuable diagnostic measure for predicting auditory nerve survival.

Influence of Stimulus Characteristics on AEPs

The acoustically-evoked CAP represents the synchronous firing of multiple auditory neurons (Goldstein and Kiang, 1958). The click-evoked CAP has also been called the whole nerve action potential (e.g. Teas et al., 1962; Dolan et al., 1983) because clicks, which have broadband acoustic spectra, theoretically trigger firing in the majority of auditory nerve fibers along the cochlear partition (assuming that the frequency response of the transducer does not truncate the bandwidth of the stimulus). However, recordings in cat (Dolan et al., 1983) and in guinea pig (Eggermont, 1976) suggested that round window CAP recordings are dominated by the summed response of basal nerve fibers even when

broadband acoustic stimuli are used since the discharge latencies of high frequency fibers are similar. Nerve fibers innervating the middle to apical regions of the cochlea may also respond to broadband stimuli; however, their discharge latencies are delayed proportionally by the traveling wave delay leading to temporal smearing and limited contributions to the CAP (Dolan, 1983).

Chirp stimuli (i.e., rising frequency tonebursts) theoretically compensate for the cochlear traveling wave delay and evoke synchronous neural firing across a large portion of the basilar membrane. The instantaneous frequency of chirp stimuli is swept from low to high frequencies according to a time constant that allows individual frequency components to arrive simultaneously at their characteristic place, leading to synchronous displacement along the basilar membrane (Shore and Nuttall, 1985). The findings of several studies (e.g. Shore and Nuttall, 1985; Fobel and Dau, 2004; Elberling et al., 2007; Elberling and Don, 2008; Don et al., 2009) and recordings in our lab (Fig. 5) indicate that chirp stimuli consistently yield larger response amplitudes than clicks and traditional toneburst stimuli.

Shore and Nuttall (1985) used a guinea pig model to compare CAPs evoked with standard chirps with rising frequency to CAPs evoked with reverse chirps with falling frequency. The frequency bandwidth and magnitude of both stimuli were equated but the frequency of the rising chirp was swept from 0.3 to 6 kHz while the frequency of the falling chirp was swept from 6 to 0.3 kHz. The time constant dictating the instantaneous frequency was determined with the frequency-place map data for guinea pig from Greenwood (1961). The falling frequency chirps were expected to induce neural firing that was more temporally disperse than for rising frequency chirps since the falling chirps began with high frequency energy that would trigger firing in the base before the low frequency energy reached the apex. Shore and Nuttall's (1985) results showed that the N_1 component of CAPs evoked at low stimulus levels (15 dB above CAP threshold) with rising frequency chirps was significantly more narrow and larger in amplitude than N_1 of CAPs evoked with falling frequency chirps at low levels suggesting that the rising chirps triggered more synchronous firing than falling frequency chirps. In a study in human participants with a similar experimental design, Chertoff et al. (2010) also found that rising frequency

chirps evoked larger CAPs than both falling frequency (i.e., reverse) chirps and traditional click stimuli of equivalent magnitude and spectral bandwidth.

Other researchers (e.g. Dau et al., 2000; Wegner and Dau, 2002; Fobel and Dau, 2004; Elberling et al., 2007; Elberling and Don, 2008) have tested the utility of chirp stimuli for improving the signal to noise ratio of ABR recordings. For example, Dau et al. (2000) recorded ABRs in 10 human participants with normal hearing with a chirp stimulus that was designed based on the cochlear model of De Boer (1980) and the frequency-place map data of Greenwood (1990). De Boer's (1980) model provided an equation for instantaneous phase based on the velocity of the traveling wave in the fluid-filled cochlea. Greenwood's (1990) data allowed place along the basilar membrane to be matched to its characteristic frequency. The results of Dau et al. (2000) indicated that wave V amplitude of ABRs evoked with chirps was significantly larger than the wave V amplitude of ABRs evoked with clicks when the sensation level of both stimuli were equated by the participants. The enhanced wave V amplitude for chirp-evoked ABRs was more pronounced at relatively low levels (e.g. 10-40 dB SL re: ABR threshold). This observation both suggests that chirp stimuli could improve threshold detection and that the time constant governing the instantaneous phase of chirps may need to be adjusted according to stimulus level. Don et al. (2009) also suggested that the ideal chirp design would account for individual variations in cochlear anatomy.

Fobel and Dau (2004) also measured chirp-evoked ABRs and confirmed that chirp stimuli yielded larger wave V amplitudes than click stimuli. In addition to using the chirp stimulus with the design described by Dau et al. (2000), Fobel and Dau (2004) compared the ABRs evoked with two other chirp stimuli; one derived from basilar membrane delay data based on stimulus frequency OAE measures from Shera and Guinan (2000), and another chirp with its instantaneous frequency derived from wave V latencies from toneburst ABR data from Neely et al. (1988). Fobel and Dau (2004) found that the most effective chirp stimulus (i.e., chirp that produced largest wave V amplitude) was the chirp designed with the toneburst ABR latency data. At low stimulus levels, the wave V amplitude of ABRs evoked with this

chirp design was triple the size of those evoked with click stimuli. Fobel and Dau (2004) interpreted this finding to suggest that chirps designed with electrophysiological measures may be superior to those designed with OAE data since electrophysiological data essentially involve both the mechanical and neural-related delays of the cochlea.

Elberling et al. (2007) have also found chirp stimuli to be effective in increasing the signal to noise ratio and reducing response detection times for recordings of the auditory steady-state response (ASSR) at low and moderate stimulus levels (30 and 50 dB nHL, respectively). Elberling and Don (2008) and Don et al. (2009) compared amplitudes of ABRs obtained with various chirp stimuli to ABR amplitudes derived with the stacked-ABR technique (Don et al., 2005) that involves click stimuli and high-pass masking noise. Using a stimulus level of 50 dB nHL, Elberling and Don (2008) found that the amplitude of chirp-evoked ABRs was nearly equivalent to the amplitude of stacked ABRs. Don et al. (2009) indicated that an ABR recording protocol using chirp stimuli could detect small acoustic tumors with a specificity of 85% with sensitivity set at 95% and required approximately 1/6 the testing time needed for a stacked-ABR protocol.

Masked AEPs

The use of chirp stimuli to evoke AEPs has been described as a form of "input compensation" for the cochlear traveling wave delay while the use of masking to isolate particular regions of neural activity has been called "output compensation" (Don et al., 2009). The stacked-ABR technique is a well known example of using masking noise to compensate for the temporally disperse neural output triggered by click stimuli. The stacked-ABR described by Don et al. (2005) represents the sum of five derived-band ABR waveforms that have been temporally aligned according to the latency of wave V. The responses are called derived-band ABRs because they represent the difference waveform resulting from subtracting a masked ABR from an unmasked click-evoked ABR. The masked ABRs are recorded during simultaneous masking with broadband noise that is high-pass filtered with five different cutoff frequencies representing octave intervals between 0.5 and 8 kHz. Don et al. (2005) tested the stacked-

ABR protocol in a group of 54 patients that either had an acoustic tumor less than one centimeter in size or had a tumor that was not detected by a standard ABR protocol involving wave V latency comparisons. Relative to MRI detection of the tumor, the stacked-ABR technique identified 100% of the tumors with a specificity of 50%. With a slightly lower sensitivity of 95%, the technique reached a specificity of 88%.

An earlier study by Teas et al. (1962) described the use of band-pass masking noise to derive narrow-band CAPs in guinea pig. Teas and colleagues used intracochlear electrodes to record CAPs to click stimuli during simultaneous masking with narrow bands of white noise with six different center frequencies. Their results indicated that narrow-band CAPs varied in peak amplitude and latency but summed to equal the unmasked CAP response. In two similar studies, Bone et al. (1972) and Prijs and Eggermont, (1981) used high-pass noise to derive narrow-band CAPs to clicks recorded from the round window in rat and guinea pig. Similar to the findings of Teas et al. (1962), they found that N_1 amplitude and N_1 latency varied proportionally with the high-pass cutoff frequency. The results of Bone et al. (1972) made them optimistic that the high-pass masking technique could be incorporated with electrocochleography protocols to obtain a location-specific diagnosis of cochlear pathology in human patients.

The utility of a high-pass masking paradigm in CAP and ABR recordings in animal and human participants has been examined in many studies (e.g., Crowley et al., 1972; Elberling, 1974; Eggermont, 1976; Spoor et al., 1976; Zerlin and Naunton, 1976; Don and Eggermont, 1978; Don et al., 1979; Shore and Nuttall, 1985; Wegner & Dau, 2002). The study of Elberling (1974) provided an estimate of the traveling wave velocity in humans based on the latencies of CAPs evoked with high-level clicks (95 dB peak equivalent SPL) during simultaneous masking with broadband noise high-passed at octave intervals between 0.5 and 8 kHz. Eggermont's (1976) work included transtympanic CAP recordings in human participants and round window CAP recordings in guinea pig. Similarities between the response areas constructed with derived-band amplitudes for humans and those constructed for guinea pigs were interpreted by Eggermont (1976) to suggest that the results of animal experiments involving round-

window CAP recordings may generalize to human patients. Don et al. (1979) applied the high-pass masking technique to click-evoked ABR recording protocols with the goal of obtaining an estimate of the behavioral audiogram in humans. Their results from three patients with different audiometric configurations (e.g., 4 kHz notch, rising low frequency, and flat) suggested that narrow-band ABR thresholds matched behavioral thresholds reasonably well (e.g., within 5-15 dB). Don et al. (1979) also detailed several potential drawbacks and limitations of clinical application of the technique including long test-time and the likely mismatch between electrophysiologic thresholds and audiometric thresholds in patients with retrocochlear tumors and severe low frequency hearing loss.

Parker and Thornton (1978 a, b, c) expressed concern as to the validity of inferring regional cochlear activity from derived-band ABRs recorded from the scalp. However, after comparing derived-band latencies from ABRs recorded in normal hearing human participants to published estimates of the traveling wave velocity, the authors concluded that the derived band technique seemed to be valid (Parker and Thornton, 1978 c). Evans and Elberling (1982) also designed an experiment to validate the use of the high-pass masking technique for deriving narrow-band CAP responses. In cat, they recorded click-evoked single-fiber activity and round window CAPs simultaneously during high-pass noise masking at various cutoff frequencies. Decreases in single-fiber activity, quantified with post-stimulus time histograms, coincided directly with decreases in CAP amplitude suggesting that a high-pass masking paradigm could provide an accurate survey of regional neural firing along the basilar membrane.

The use of notched-noise in combination with toneburst stimuli has also been investigated by several researchers (e.g., Picton et al., 1979; Stapells and Picton, 1981; Stapells et al., 1990; Stapells et al., 1995). The primary goal of these investigations was to determine if notched noise could reduce the frequency spread of brief tonebursts and allow accurate estimates of frequency-specific hearing thresholds. The data of Picton et al. (1979) suggested that the notched-noise protocol yielded toneburst ABR thresholds that were within 20 dB of behavioral pure-tone thresholds. A similar study by Stapells et al. (1995) of 34 children with normal hearing and 54 children with sensorineural hearing loss indicated

that the large majority of ABR thresholds estimated with tonebursts centered in notched-noise were within 15-30 dB of behavioral thresholds. Picton et al. (1979) also acknowledged concern regarding the possible upward spread of masking from the acoustic energy from the low frequency side of the notched noise. The upward spread is likely most pronounced when using high-level toneburst stimuli that require higher noise levels to provide sufficient masking of the toneburst side lobes. This very concern lead to an early change in the experimental design of this study from using high-level tonebursts embedded in notched noise to high-level chirps with a high-pass masking paradigm.

Gentamicin-Induced Impairment of OHCs

The effects of gentamicin on cochlear hair cells has been studied in chicks (Husmann et al., 1998), pigeons (Müller and Smolders, 1998), mice (Heydt et al., 2004), and gerbils (Wanamaker et al., 1998; Sheppard et al., 2004; Suryadevara et al., 2009) by applying gentamicin directly to the round window. The use of a drug delivery vehicle (e.g. Gelfoam®) has also been shown to produce hair cell damage more reliably and more extensively than directly dripping gentamicin into the round window niche in chicks (Hussman et al., 1998) and gerbils (Sheppard et al., 2004). Other studies (e.g., Ylikoski, 1974; Ylikoski et al., 1974; Szymanski et al., 1994) have used systemic injections of gentamicin or other aminoglycoside antibiotics to induce hair cell pathology in animal subjects. However, the systemic dosages required to induce substantial hair cell pathology were frequently toxic and/or lethal to the animals. Round window application of gentamicin prevents systemic toxicity and also allows the opposite ear to serve as a control for anatomical comparisons (e.g., Husmann et al., 1998).

Husmann et al. (1998) used 11-day old chicks in their experiment and found that directly dripping gentamicin into the round window niche resulted in either minimal damage to the cochlea (~5-10% of length of cochlea) or no visible damage at all. In contrast, when the same amount of gentamicin was infused into a Gelfoam ® pledget and placed on the round window, hair cell damage was observed along 50-100% of the length of the chick cochleae. Husmann et al. (1998) also observed that a gentamicin dose of 0.5 mg (500 µg) and an exposure time of only 30 minutes resulted in damage across 50% of the length

of the cochlea. Higher doses (e.g., 1.0 mg) and exposure times as long as 5 days resulted in 80-90% of the length of the cochlea being damaged. Sheppard et al. (2004) compared Gelfoam-based delivery vehicles to other vehicles (i.e., hyaluronic acid and fibrin) in gerbils and found that the Gelfoam-based vehicle produced the most homogenous damage across animals. Specifically, gerbils that received two weeks of gentamicin exposure via Gelfoam® delivery vehicles, sustained hair cell damage throughout 90-100% of the cochlea while other vehicles resulted in less complete and more variable damage.

Müller and Smolders (1998) analyzed ABR thresholds and hair cell anatomy in pigeons following gentamicin administration to the round window via Gelfoam ®. Data from 21 ears that received a 0.5 mg dose of gentamicin suggested that ABR threshold shifts and hair cell morphology changes occurred within five days post-exposure. ABR thresholds for middle and high frequency stimuli shifted 40-70 dB while the thresholds for low frequency stimuli shifted by only 10-20 dB. Scanning electron microscope images of the hair cell anatomy showed nearly complete destruction of hair cells across the entire length of the cochlea (i.e., basilar papilla) by seven days after gentamicin exposure.

Heydt et al. (2004) used mice (n = 82) to determine the effect of round-window application of gentamicin (delivered via Gelfoam®) on OHCs and IHCs. Their data indicated that a 25 µg dose of gentamicin resulted in OHC damage throughout the basal and middle cochlear turns but minimal IHC damage after 24 hours. Sheppard et al. (2004) used a much higher gentamicin dose of 445 µg in gerbil with a two-week survival period and observed nearly equal damage to OHCs and IHCs. The study of Suryadevara et al. (2009) included a group of two gerbils that were exposed to gentamicin-soaked fibrin clots on the round window. Fibrin is described as gel-like material that is made by combining bovine-derived fibrinogen and thrombin. Two weeks post-application of the gentamicin, histologic observations indicated that 65% of OHCs and 49% of IHCs remained intact.

Although the data of Sheppard et al. (2004) and Suryadevara et al. (2009) indicate that long-term (e.g., 2 weeks) exposure to gentamicin results in damage to the OHCs and IHCs in gerbil, observations over shorter time increments (e.g., hours to days) in gerbil (Wanamaker et al., 1998), guinea pig (Ylikoski

et al., 1974), and mouse (Heydt et al., 2004) have indicated that gentamicin exposure damages OHCs before IHCs. Ylikoski et al. (1974) used light microscopy to sequentially observe the effect of gentamicin and kanamycin on the inner ear structures of guinea pig. In the majority of 42 ears, Ylikoski et al. (1974) noted that SGCs and IHCs remained normal in appearance when OHC damage was widespread.

Wanamaker et al. (1998) summarized the findings of several animal studies that have investigated the time-course of the ototoxic effects of gentamicin and other aminoglycosides. The time-course of aminoglycoside effects has largely been determined by studies using systemic injections of aminoglycosides followed by blood and perilymph samples. Within 3-5 hours post-injection, peak levels of aminoglycosides are detected in the perilymph of the cochlea. The drug is also detectable in the endolymph but at lower levels and after more time post-injection. The half-life of aminoglycosides, or the rate at which they are eliminated, ranges from 3 to 15 hours post-injection.

The mechanisms behind the ototoxic effects of aminoglycosides have been investigated at the molecular level by several investigators. Williams et al. (1987) and Blanchet et al. (2000) isolated OHCs from guinea pig and studied the effects of gentamicin in vitro. The key finding of both studies was that gentamicin displaced calcium cations from OHCs suggesting a direct influence of aminoglycosides on three OHC properties controlled by calcium; membrane stability, excitability, and slow motility. Williams et al. (1987) found that once gentamicin crossed the OHC membrane, it proceeded to bind with phospholipid elements that maintain the integrity of the cell membrane. This interference would then likely disrupt hydrolysis processes that are necessary for cell survival. Li and Steyger (2009) reviewed several other studies that identify non-selective cation channels and stereocilia tip channels as likely OHC entry points for gentamicin. Other possible entry points into the cochlea include marginal cells of the stria vascularis, endothelial cells of the lateral wall, and the tight-junction cells of Reissner's membrane and the basilar membrane (Li and Steyger, 2009).

Li and Steyger (2009) also described a synergistic effect of exposure to aminoglycosides and noise exposure. Brown et al. (1978) investigated the effect with a 7-day experiment in guinea pig that

involved daily subcutaneous injections of neomycin (200 mg/kg) and a daily 10-hour exposure to high-level (115 dB SPL) white noise (bandwidth = 0.5-10 kHz). Compared to a neomycin-only control group that experienced a 17 dB shift in CM thresholds and a noise-only group that experienced a 16 dB shift in CM thresholds, a mean shift of 62 dB was observed for the neomycin plus noise group. Histological comparisons indicated that the neomycin-only group had 25% OHC loss while the neomycin plus noise group averaged 100% OHC loss. Brown et al. (1978) also pointed out that IHC loss for the neomycin-only group was minimal while the neomycin plus noise group neared 100% IHC loss.

Influence of OHC Pathology on High-Level AEPs

Determining the influence of OHC damage on the amplitude of CAPs evoked with high-level chirp stimuli was the focus of the second experiment of this study. These data are novel since published studies that have measured CAPs after administration of ototoxic agents have focused on response threshold instead of response amplitudes. For example, Szymanski et al. (1994) analyzed CAP (and ABR) thresholds following a 14-day period of subcutaneous gentamicin injections in one group of pigmented gerbils and another group of albino gerbils. They found that CAP threshold shifts were most pronounced for high frequency stimuli and significantly larger for albino gerbils than for pigmented gerbils following gentamicin treatment. This influence on threshold was anticipated since gentamicin is known to induce OHC pathology. Data for CAP amplitude for suprathreshold stimuli were not reported.

Dallos and Harris (1978) examined the characteristics of single-unit recordings from chinchilla with kanamycin-induced OHC damage. The characteristics of post-stimulus time histograms (e.g., latency, spontaneous rate, and time pattern) for animals with OHC pathology did not show any significant change suggesting that IHCs with which the afferent neurons synapse were functioning normally. Frequency threshold curves (FTC) obtained for units within the region of the OHC lesion exhibited truncated tips consistent with an elevated discharge threshold at the units' characteristic frequency. The tail segments of the FTCs for units within regions of OHC damage were essentially equivalent to FTCs

for normal units suggesting that when the stimulus was sufficiently intense, IHCs triggered normal neural firing independent of OHC action.

Eggermont (1977) obtained CAP tuning curves from transtympanic recordings in human patients using toneburst stimuli and tone-on-tone masking techniques. Tuning curves from patients with hearing loss were compared to tuning curves from normal hearing individuals. Patients with hearing loss exhibited broad tuning without pronounced tips but the tail segments of their tuning curves were roughly equivalent to the tail segments of tuning curves in normal hearing individuals. Eggermont (1977) commented that those patients with hearing loss classified as sensory (inferred from the presence of recruitment) had normal CAP amplitudes for high-level stimuli. This observation suggests that high-level stimuli produce enough basilar membrane displacement to depolarize IHCs and trigger afferent nerve firing.

Appendix B

Figures and Tables

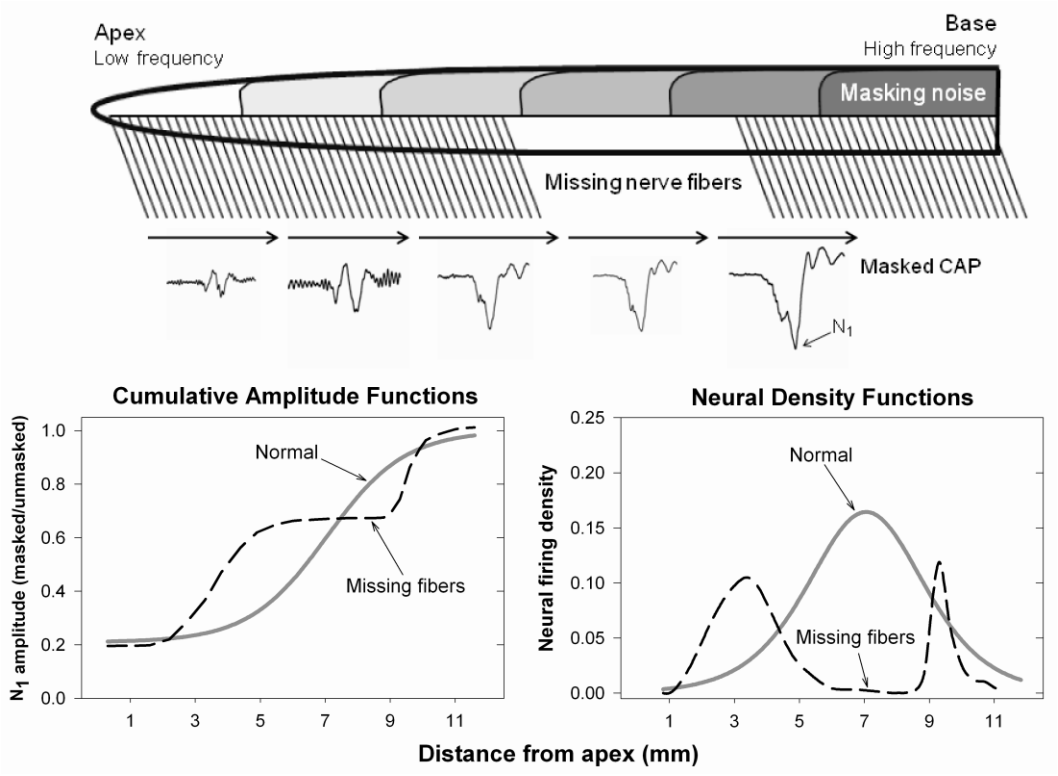

Fig. 1. Top panel: Schematic of an uncoiled cochlea illustrates the idea of using multiple bandwidths of high-pass noise to systematically limit the region of auditory nerve fibers that can contribute synchronously to CAPs evoked with high-level stimuli. Bottom left panel: Normalized N_1 amplitude would theoretically grow differently for a cochlea with missing auditory nerve fibers (dashed line) than for a normal cochlea (solid line). Bottom right panel: Derivatives of the respective cumulative amplitude functions (CAFs) yield neural density functions (NDFs) that theoretically reveal the distribution of viable nerve fibers contributing to the CAP.

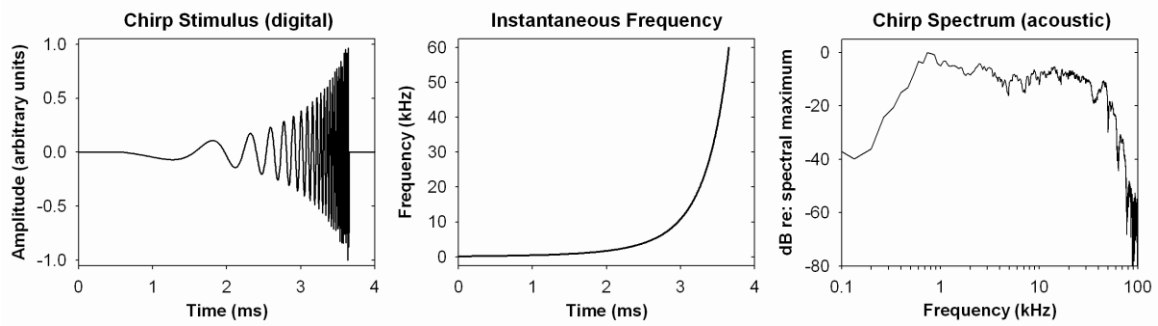

Fig. 2. Left panel: Digital waveform of gerbil-tailored chirp that rises in frequency and amplitude over a duration of 3.06 ms. Middle panel: Instantaneous frequency of chirp stimulus is equivalent to the inverse of cochlear traveling wave delay in gerbil (estimated with gerbil CAP latency data from Earl and Chertoff, 2010). Right panel: Acoustic spectrum of chirp stimulus shows relatively flat spectral energy between 1 and 60 kHz, spanning nearly the entire range of gerbil hearing.

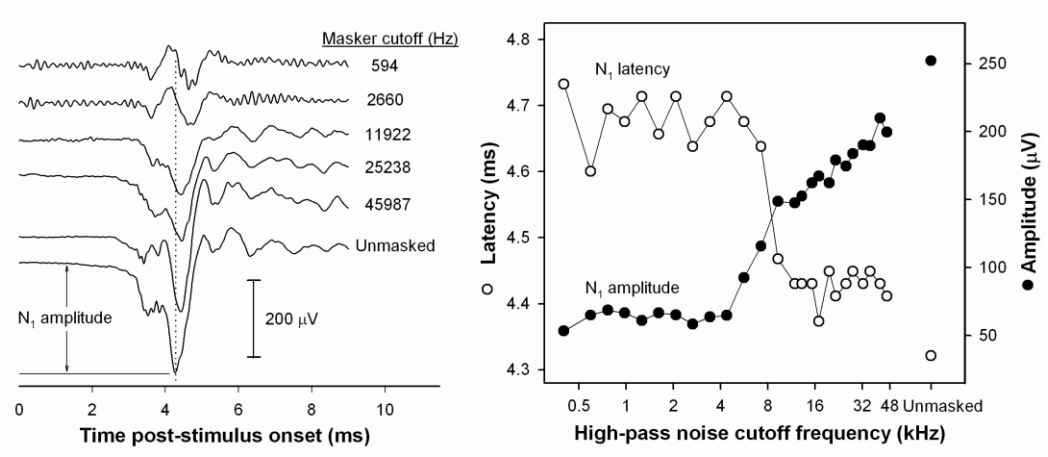

Fig. 3. Left panel: Representative unmasked and masked CAP waveforms from a normal-hearing gerbil illustrate the trend of decreasing N_1 amplitude and increasing N_1 latency as the high-pass noise masker cutoff frequency decreases. Right panel: Representative raw data for N_1 amplitude (filled circles, units on right ordinate) and N_1 latency (open circles, units on left ordinate) for all 25 masking conditions. Unmasked values represent the mean of four unmasked CAP recordings.

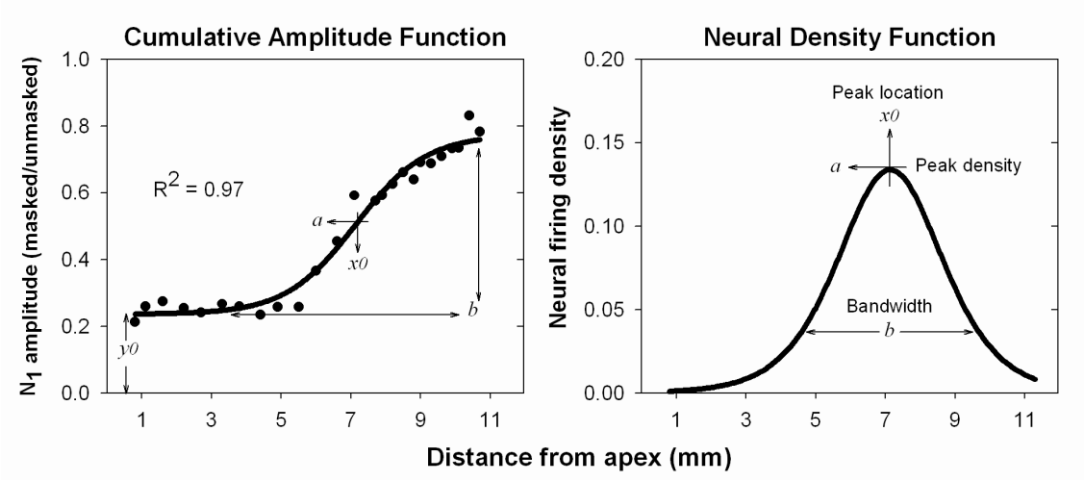

Fig. 4. Left panel: Normalized N_1 amplitude data (filled circles) plotted as a function of distance from apex (converted from masker cutoff frequency with frequency-place map for gerbil from Müller, 1996). The cumulative amplitude function (CAF), shown with thick line along with its corresponding coefficient of determination (R^2), is obtained by fitting the data with a four-parameter (*a*, *b*, *x0*, *y0*) sigmoid function. Right panel: The neural density function (NDF; thick line) is obtained by using the CAF parameters to solve the analytical derivative of the CAF (Equation 2) for distance from apex (*x*). The peak location is given by parameter *x0* and the bandwidth is defined as the distance spanned by the inner 2/3 of the area under the curve (calculated by multiplying peak density by 0.3413 and finding the difference between the corresponding distance values).

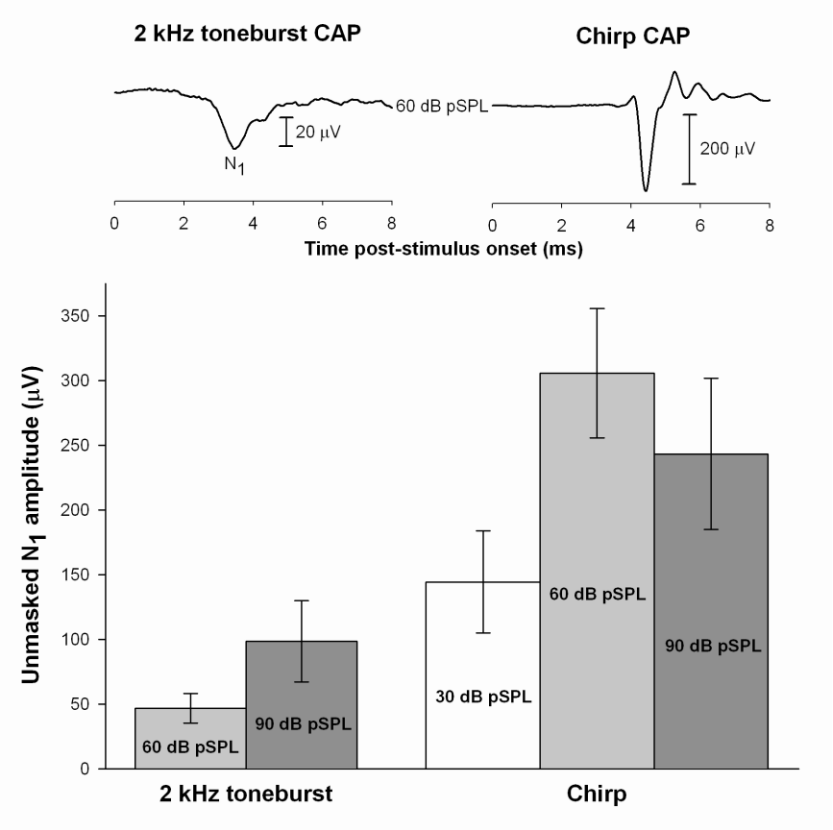

Fig. 5. Top panel: A representative CAP evoked with 2 kHz tonebursts at 60 dB pSPL (top left) is nearly 10 times smaller in magnitude than a CAP evoked with chirps at the same level (top right). Bottom panel: Comparison of unmasked N_1 amplitudes illustrates that chirps at 60 dB pSPL produced the largest CAPs. Even chirps as low as 30 dB pSPL generated CAPs that were larger in magnitude than 2 kHz tonebursts at 90 dB pSPL. Error bars = 1 SD; n = 9 for each stimulus condition except for chirp at 30 dB pSPL where n = 4.

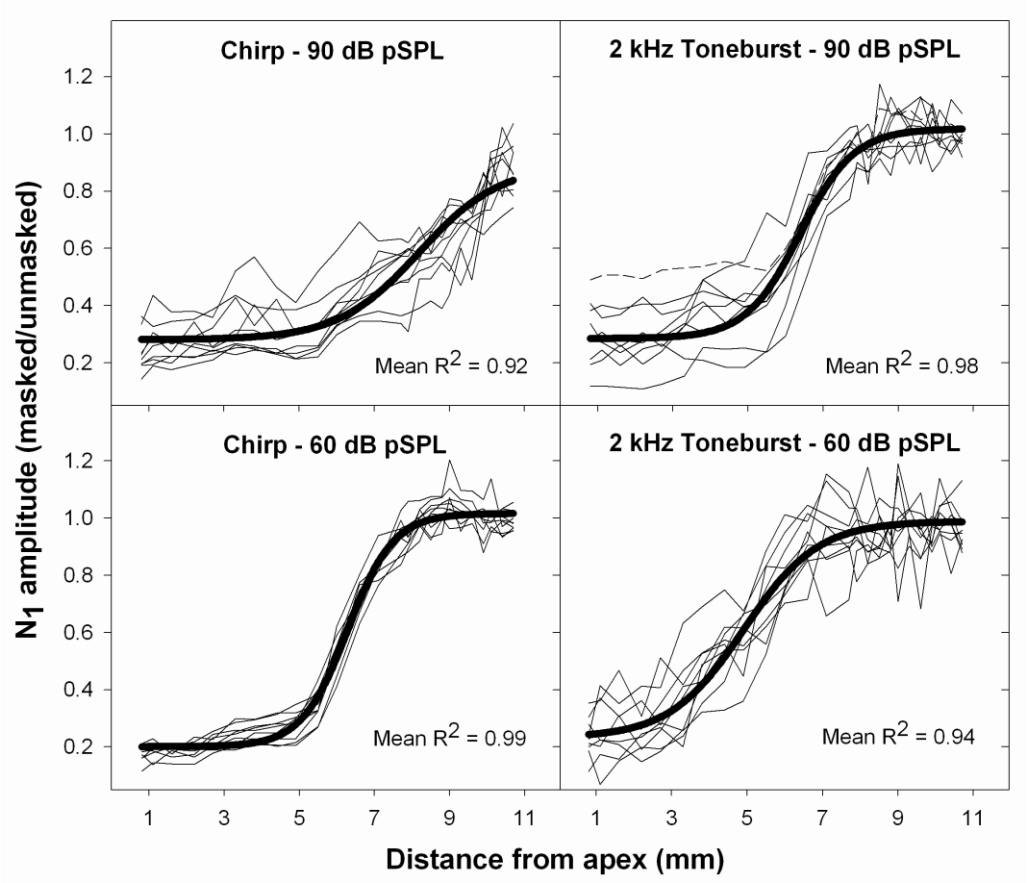

Fig. 6. Normalized N_1 amplitude data (thin lines) for nine normal-hearing gerbils (Experiment 1) with their corresponding mean CAFs (thick lines) show differences in slope and variability across stimulus type and level. The data shown with a dashed line in the upper right panel was determined to be an outlier (initial masked amplitude was more than two SD above the mean of initial masked amplitude across all stimulus conditions) and was excluded from further analysis. Mean coefficients of determination (R^2) indicate that the four-parameter sigmoid function accounts for a large majority of the variance in the data.

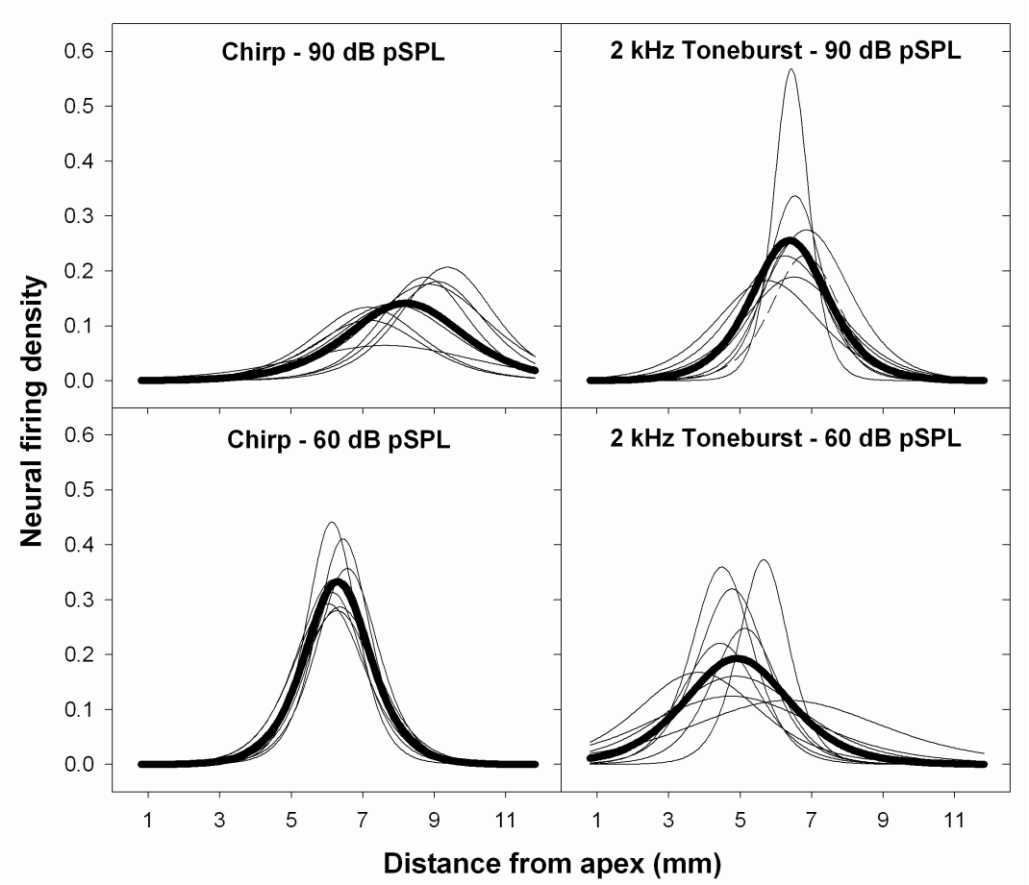

Fig. 7. Individual NDFs (thin lines) and the corresponding mean NDFs (thick lines) for the nine normal-hearing gerbils (Experiment 1) illustrate the distribution of neural firing density for each stimulus type and level combination. The individual NDF shown with the dashed line in the upper right panel represents the outlier that was described in Fig. 6.

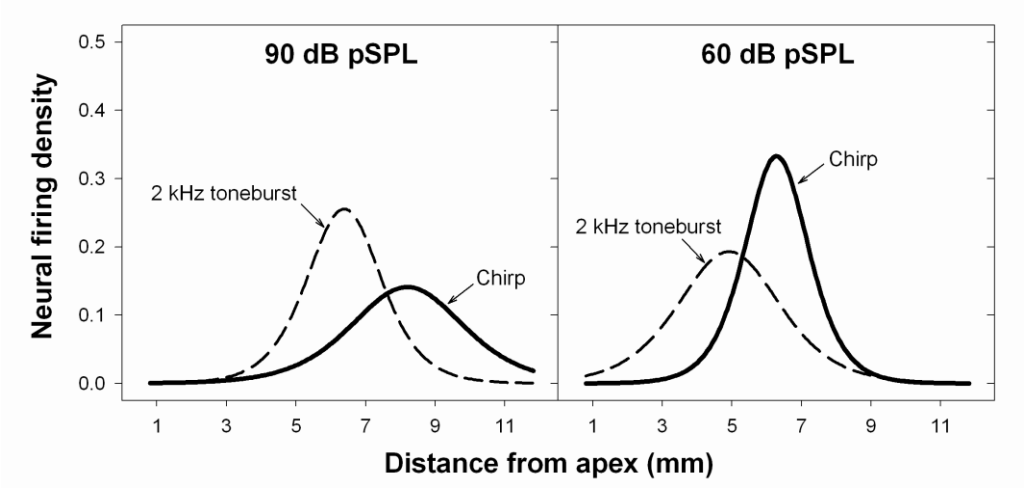

Fig. 8. Comparison of the mean NDFs for chirps (solid lines) and 2 kHz tonebursts (dashed lines) at each stimulus level reveals differences between bandwidth and peak location. See Table 1 for statistical analysis.

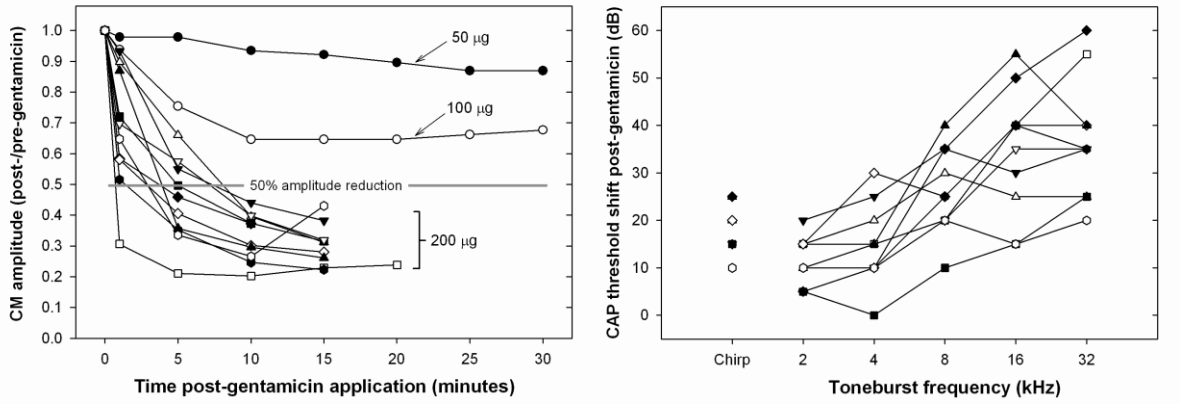

Fig. 9. Left panel: Cochlear microphonic (CM) data for the 10 gerbils in Experiment 2 indicate an exponential decrease in amplitude over a course of minutes following application of 200 µg of gentamicin to the round window niche. The CM was evoked with 16 kHz tonebursts (10 ms in duration) at 80 dB pSPL. Dose-response curves for lower gentamicin doses (50 and 100 µg) are shown for comparison. Right panel: Post-gentamicin CAP threshold data show shifts ranging from 10 to 25 dB for chirps and a general trend of increasing threshold shifts for tonebursts as stimulus frequency increases.

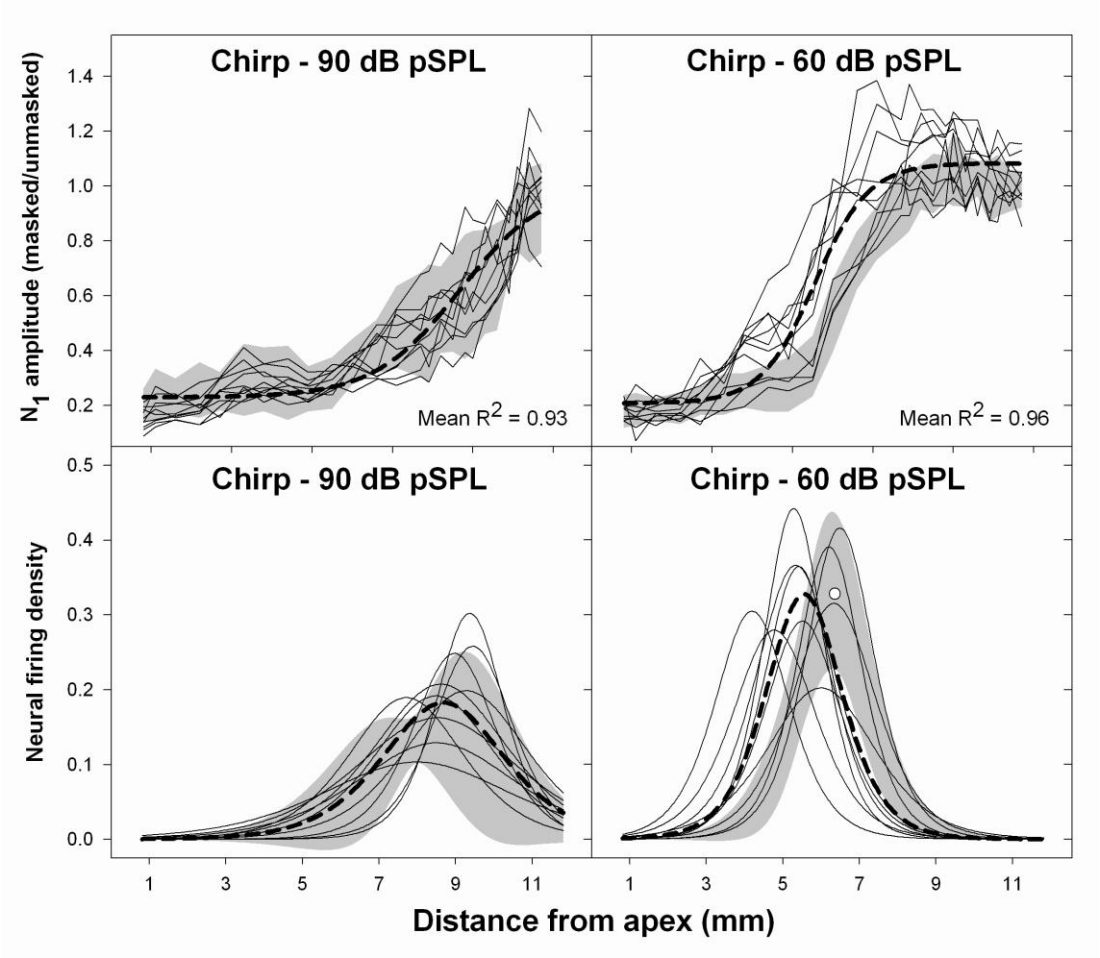

Fig. 10. Top panels: N_1 amplitude functions for 10 gentamicin-exposed gerbils (thin lines) fall within the normal range (mean +/- 2SD; gray areas) for chirps at 90 dB pSPL, whereas for chirps at 60 dB pSPL, 6 out of the 10 gentamicin-exposed animals fall outside the normal range. Thick dashed lines in the top panels represent the mean of the post-gentamicin CAFs. Mean R^2 values indicate that the four-parameter sigmoid function accounts for a large majority of the variance in the post-gentamicin data. Bottom panels: Individual NDFs for the 10 gentamicin-exposed gerbils (thin lines) with the mean NDFs (thick dashed lines) plotted against the normal ranges (mean +/- 2SD; gray areas) indicate minimal difference between the mean bandwidth and mean peak location for chirps at 90 dB pSPL. For chirps at 60 dB pSPL, mean bandwidth did not differ across groups but the mean peak location for the gentamicin-exposed group was significantly more apical than the mean peak location for the normal-hearing group (open circle). See Table 2 for statistical analysis.

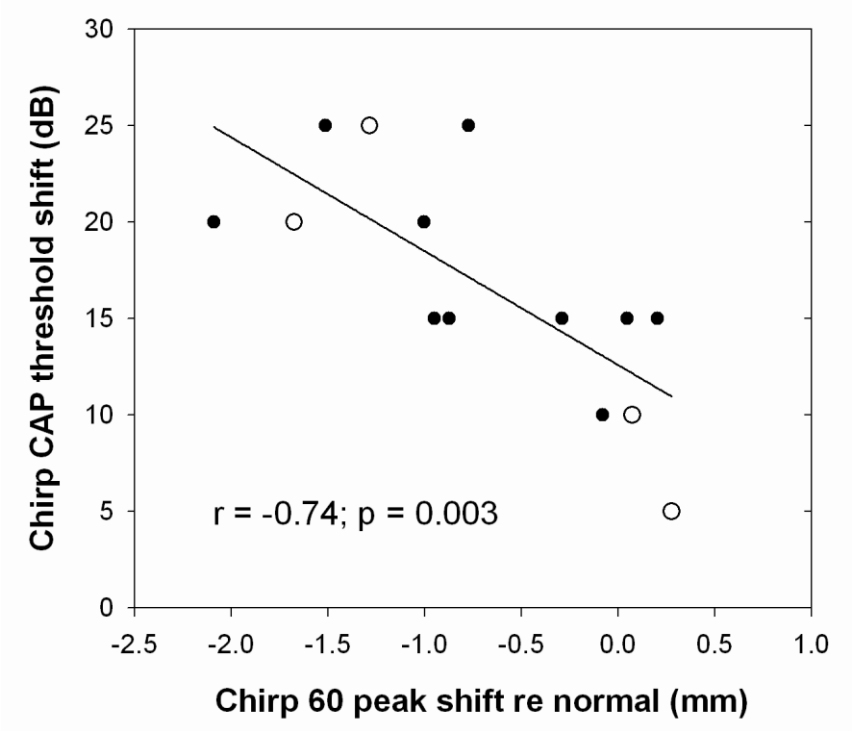

Fig. 11. Plotting the post-gentamicin shift in chirp CAP thresholds against the post-gentamicin shift in NDF peak location for chirps at 60 dB pSPL (re normal mean peak location for chirps at 60 dB pSPL) reveals a significant inverse correlation between the two variables. Negative values for peak shift indicate apical shifts re normal peak location. Filled circles (n = 10) represent the animals that met the inclusion criteria for Experiment 2. Open circles (n = 4) represent animals excluded from analysis due to progressive CAP threshold shifts during the course of data collection (two upper circles) or due to minimal chirp CAP threshold shifts following gentamicin application (two lower circles).

Table 1. Descriptive statistics and results of paired samples t-tests comparing NDF bandwidth and peak location across stimulus type at 90 and 60 dB pSPL (Experiment 1)

	Bandwidth (mm)			Peak location (mm)		
	Mean	SD†	*p*	Mean	SD†	*p*
Chirp 90 (n=8)*	4.87	1.84	0.04	8.22	1.01	0.001
Toneburst 90 (n=8)*	3.25			6.38		
Chirp 60 (n=9)	2.78	2.04	0.04	6.28	0.61	<0.001
Toneburst 60 (n=9)	4.43			4.91		

*Sample size (n) reduced to 8 for paired comparisons at 90 dB pSPL due to exclusion of outlier indicated with dashed line in upper right panel of Fig. 6
†SD, standard deviation of the paired differences

Table 2. Descriptive statistics and results of independent samples t-tests comparing bandwidth and peak location of chirp NDFs for normal vs. post-gentamicin groups at 90 and 60 dB pSPL (Experiment 2)

		Bandwidth (mm)			Peak location (mm)		
		Mean	SD	*p*	Mean	SD	*p*
Chirp 90	Normal (n=7)*	4.56	0.66	0.64	8.43	0.79	0.46
	Post-gentamicin (n=10)	4.86	1.53		8.68	0.58	
Chirp 60	Normal (n=9)	2.78	0.39	0.24	6.28	0.17	0.01†
	Post-gentamicin (n=10)	3.05	0.54		5.55	0.72	

*Sample size (n) of normal group reduced to 7 for Chirp 90 NDFs due to exclusion of two outliers (initial masked amplitude > 2 SD above the mean initial masked amplitude of all chirp conditions)
†Equal variances not assumed per Levene's Test
SD, standard deviation of the mean

Appendix C

CAP Waveforms

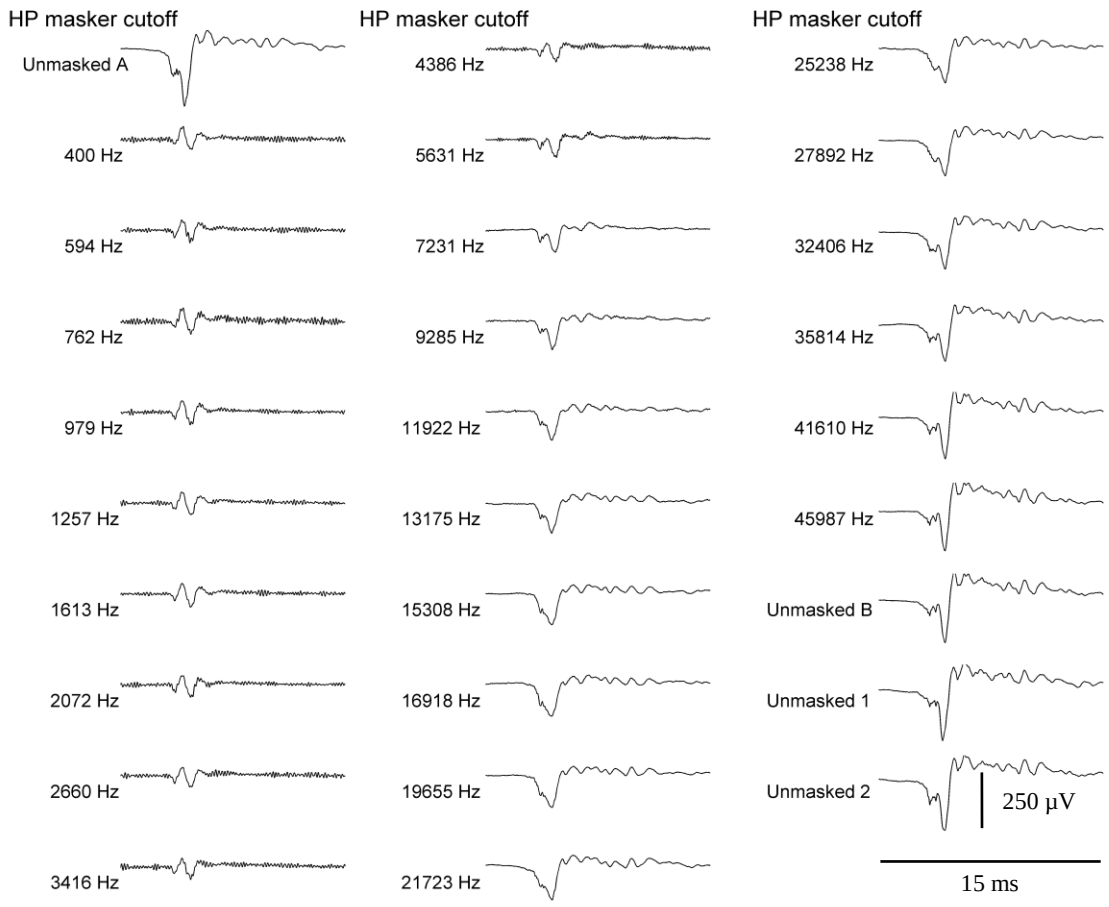

Fig. C.1. Representative masked and unmasked CAP waveforms evoked with chirps at 90 dB pSPL from a normal-hearing gerbil. High-pass (HP) masker cutoff frequencies are listed to the left of each waveform.

Normal CAPs: Chirp – 60 dB pSPL

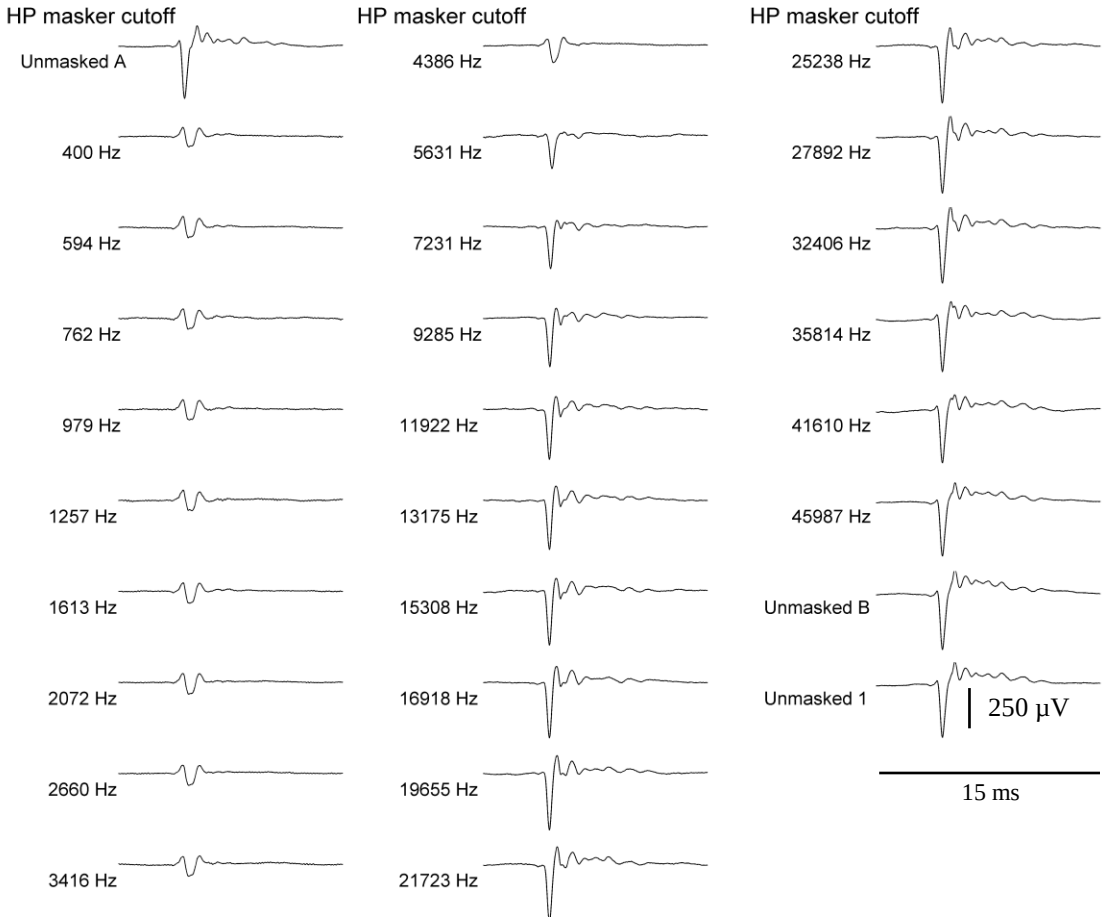

Fig. C.2. Representative masked and unmasked CAP waveforms evoked with chirps at 60 dB pSPL from a normal-hearing gerbil. High-pass (HP) masker cutoff frequencies are listed to the left of each waveform.

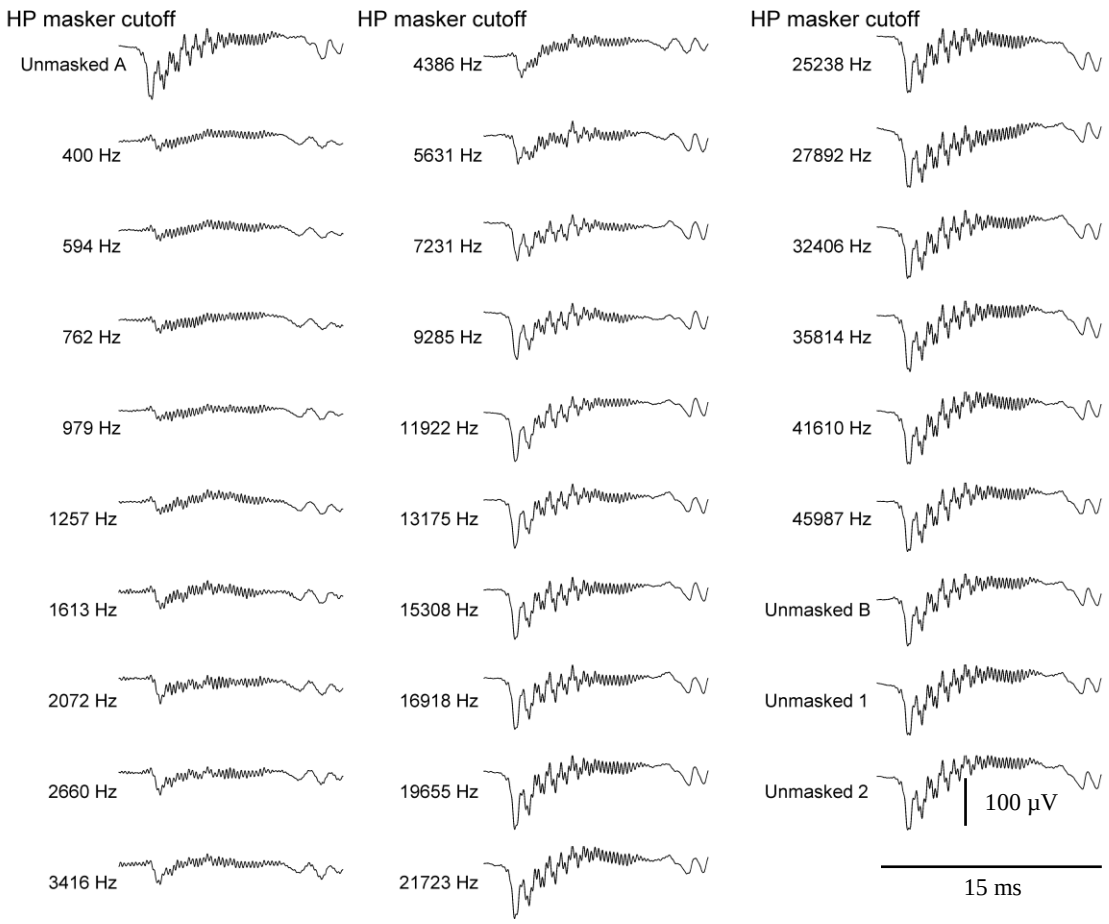

Fig. C.3. Representative masked and unmasked CAP waveforms evoked with 2 kHz tonebursts at 90 dB pSPL from a normal-hearing gerbil. High-pass (HP) masker cutoff frequencies are listed to the left of each waveform.

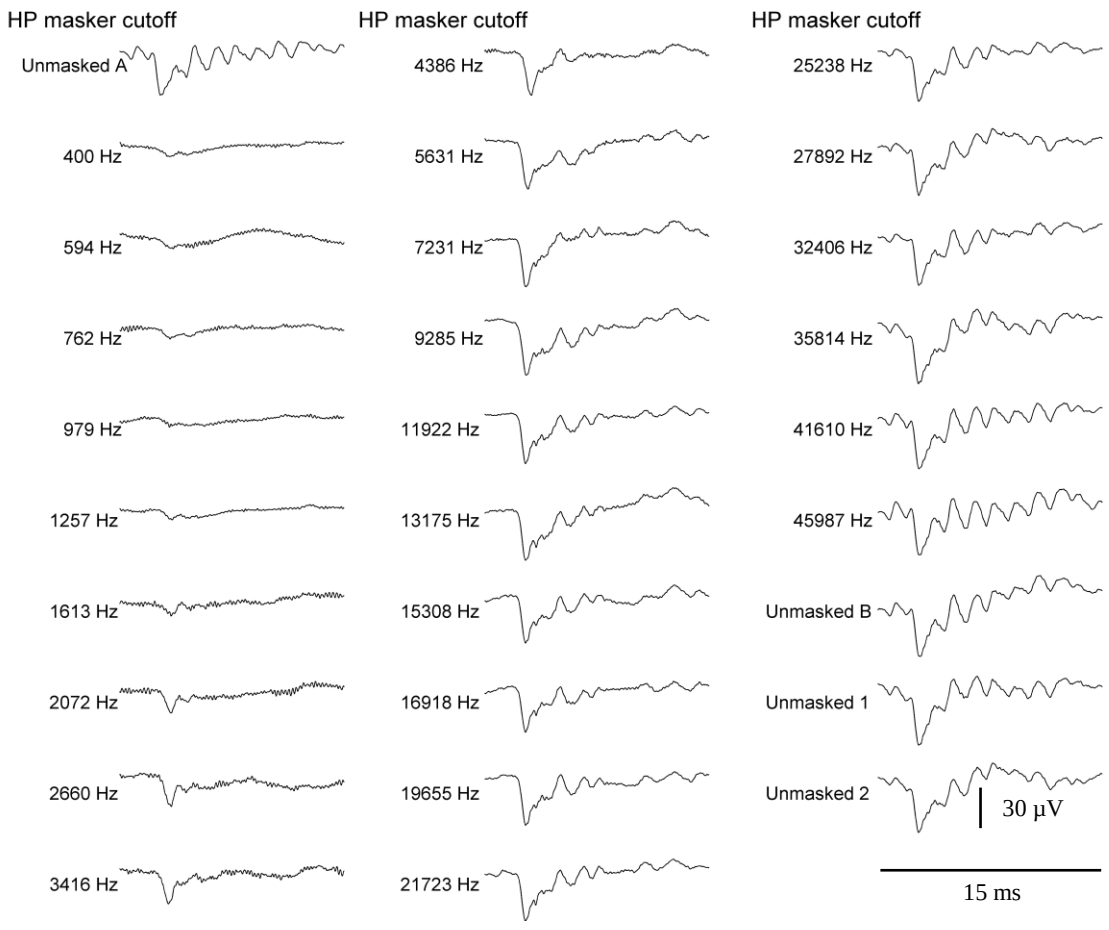

Fig. C.4. Representative masked and unmasked CAP waveforms evoked with 2 kHz tonebursts at 60 dB pSPL from a normal-hearing gerbil. High-pass (HP) masker cutoff frequencies are listed to the left of each waveform.

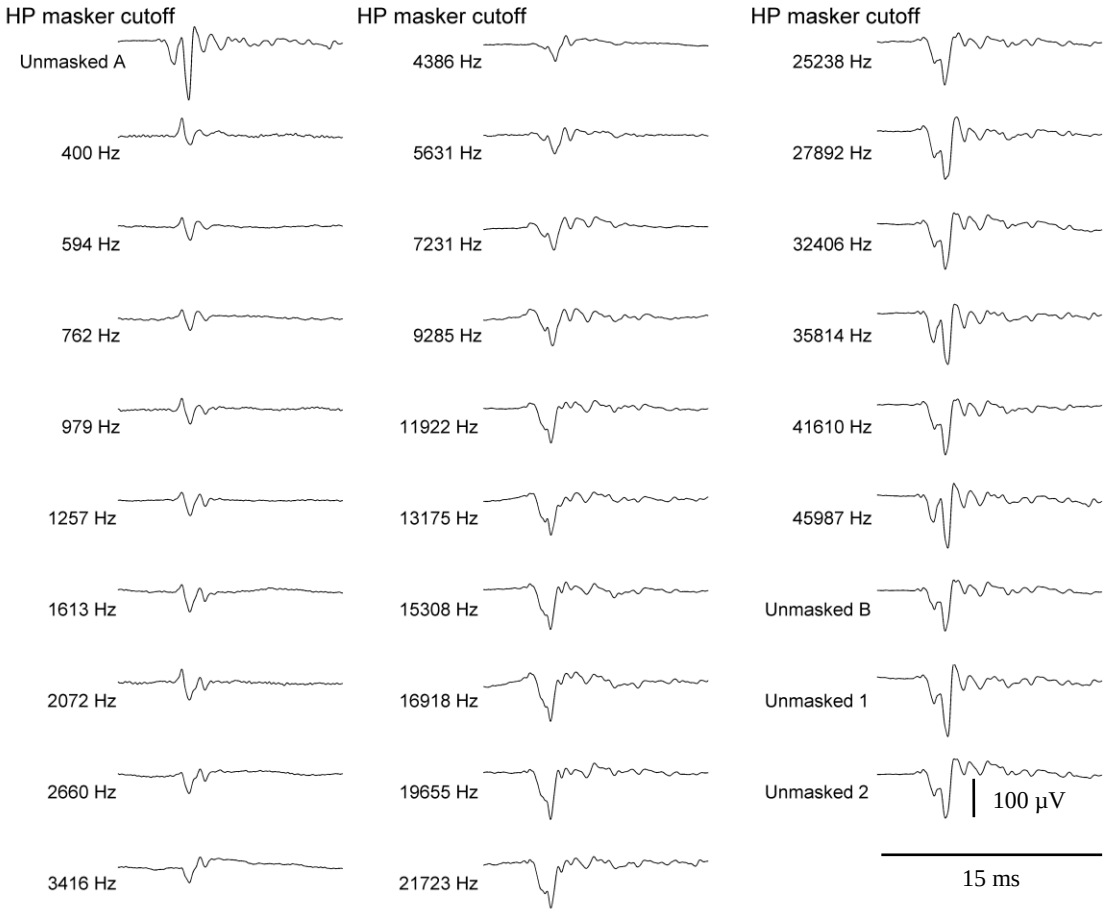

Fig. C.5. Representative masked and unmasked CAP waveforms evoked with chirps at 90 dB pSPL from a gentamicin-exposed gerbil. High-pass (HP) masker cutoff frequencies are listed to the left of each waveform.

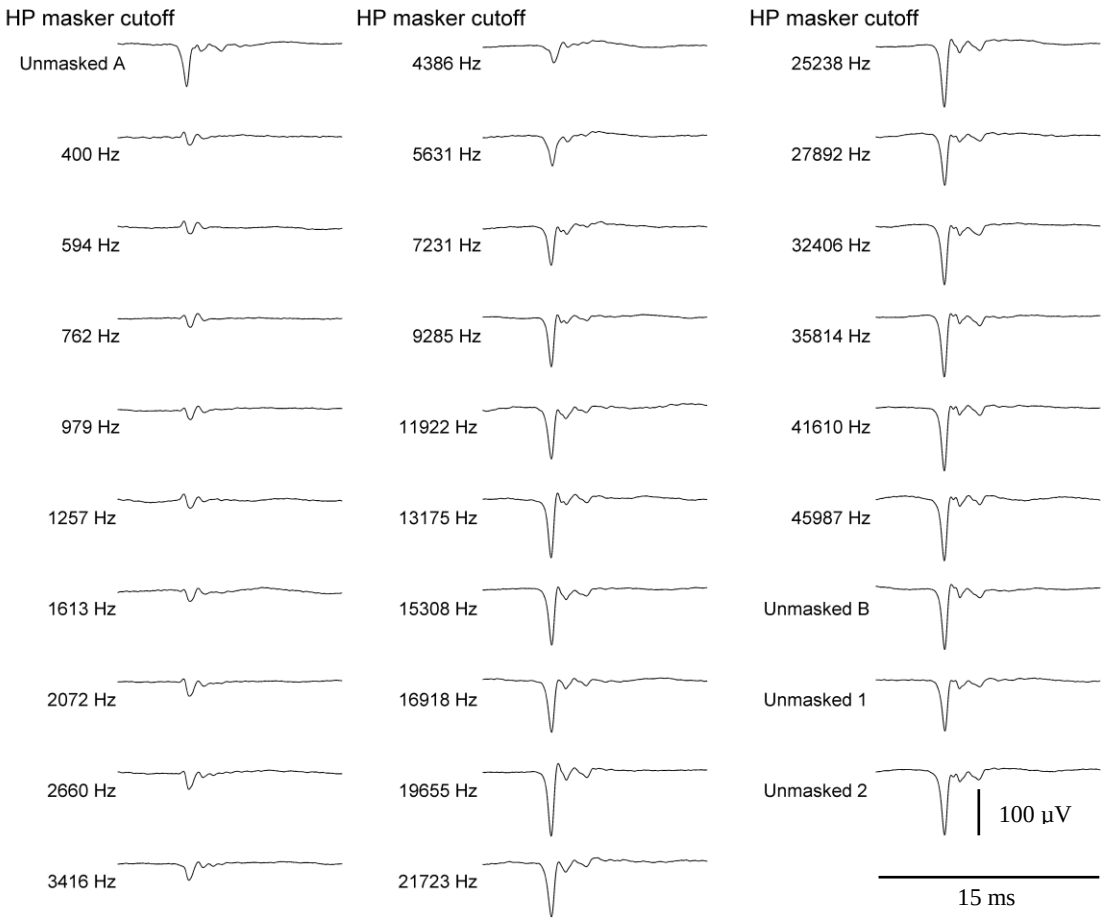

Fig. C.6. Representative masked and unmasked CAP waveforms evoked with chirps at 60 dB pSPL from a gentamicin-exposed gerbil. High-pass (HP) masker cutoff frequencies are listed to the left of each waveform.

Appendix D

Latency Analysis

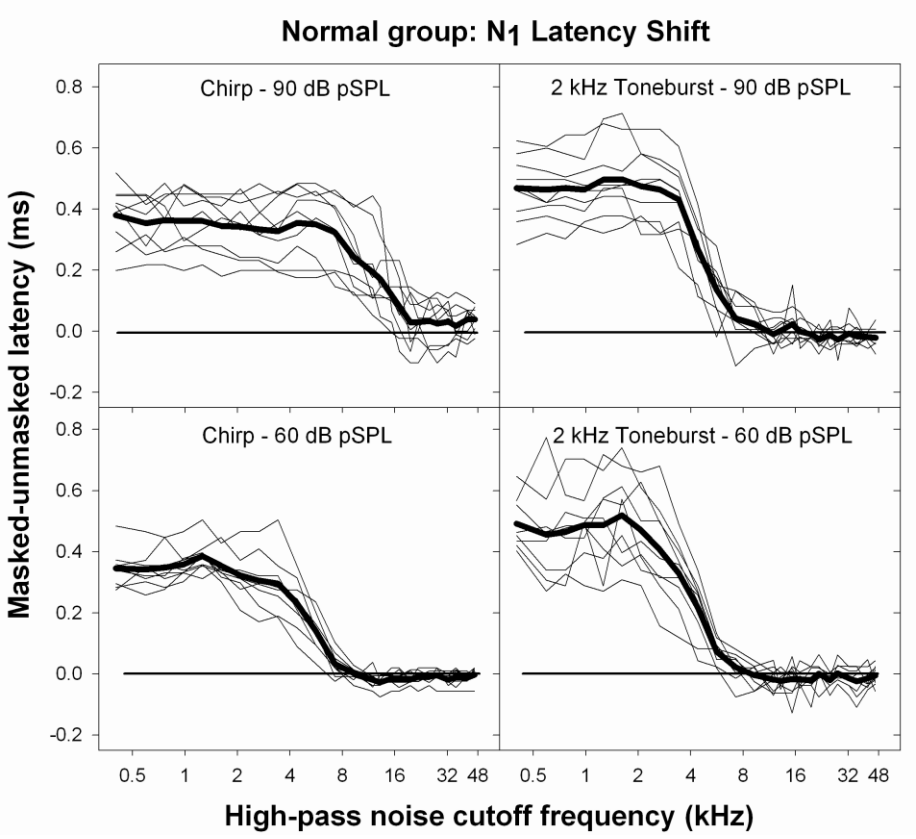

Fig. D.1. N_1 latency shift (masked-unmasked latency) plotted as a function of high-pass noise cutoff frequency for the normal-hearing group of Experiment 1. Individual animal data are shown with thin lines and the group means are shown with thick lines. The latency shift functions are generally consistent with the theory suggested by Teas et al. (1962) and the data from others (e.g. Elberling, 1974, Don et al., 1979, Evans and Elberling, 1982) that the location of synchronous neural firing for moderate and high-level stimuli is "pushed" toward the apex proportional to the high-pass noise cutoff frequency. The trends in latency shift resemble the inverse of the patterns observed for N_1 amplitude growth (Fig. 6).

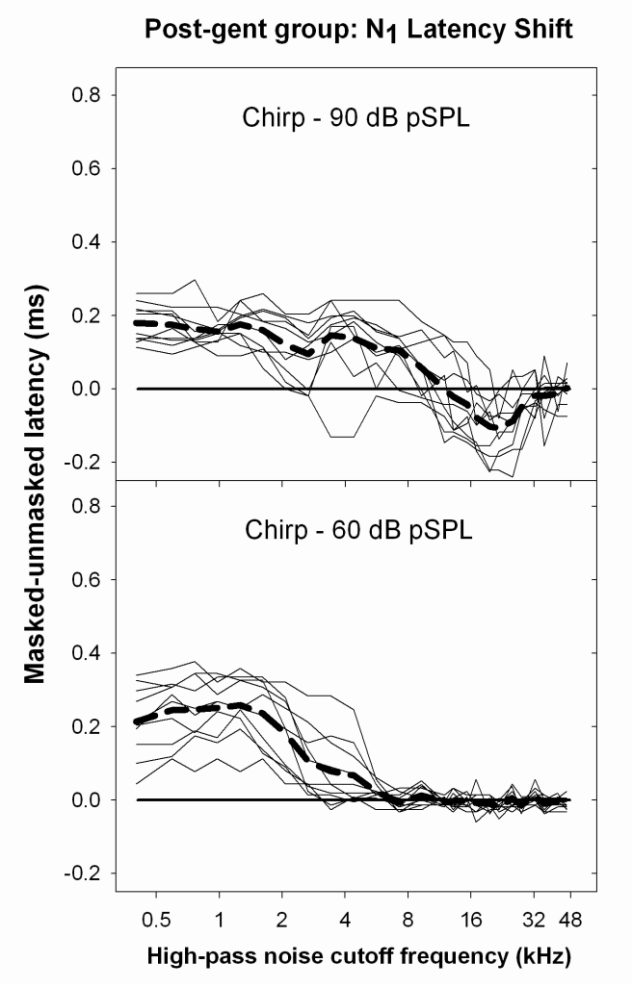

Fig. D.2. N_1 latency shift (masked-unmasked latency) plotted as a function of high-pass noise cutoff frequency for the post-gentamicin group in Experiment 2 (thin lines = individual animal data; thick dashed lines = group means) indicates smaller shifts in latency and more variability when compared to the trends in the latency data from the normal-hearing group (Fig. D.1.).

Appendix E

Alternative Analysis Method

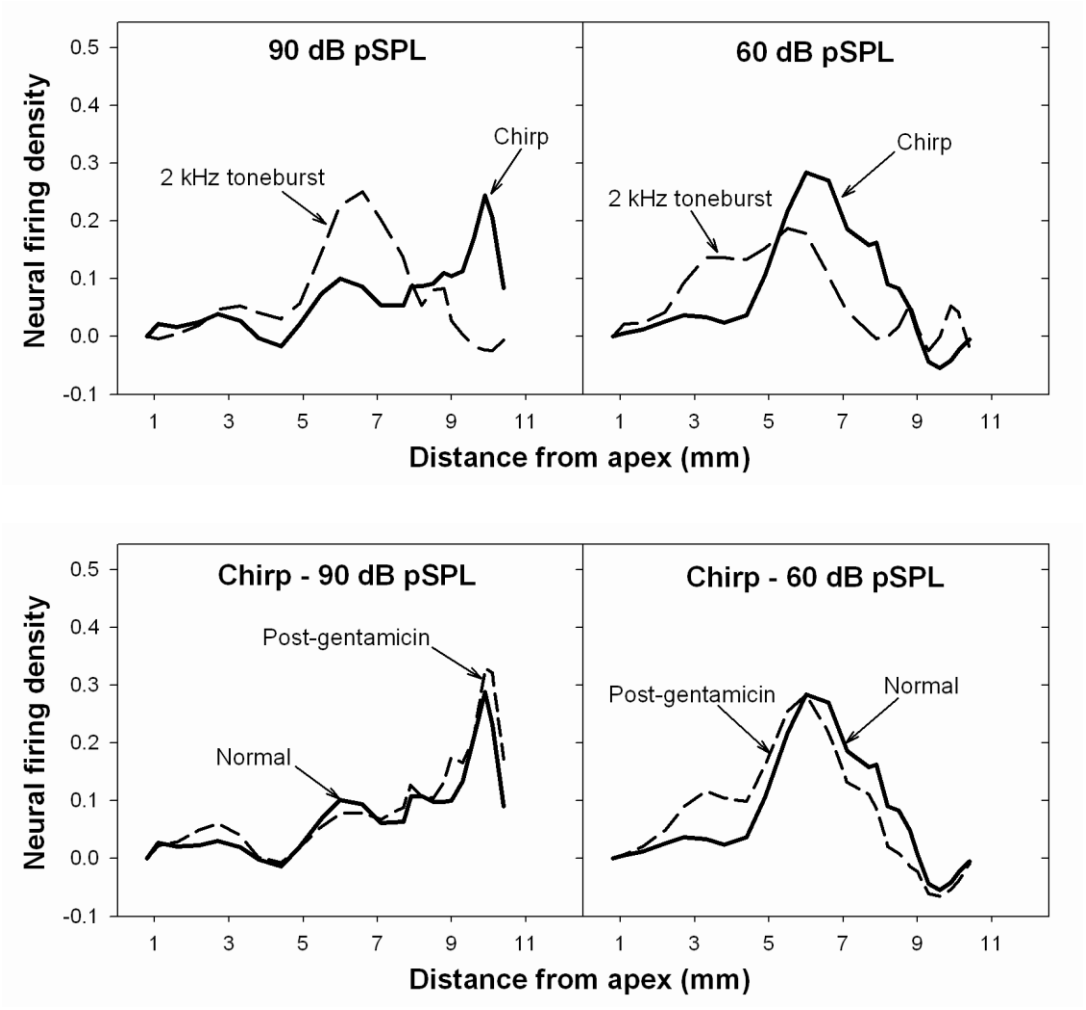

Figure E.1. An alternative method for constructing NDFs by calculating the numerical derivatives of the N_1 amplitude data (instead of taking the analytical derivative of the equation fitted to the data) preserves the "fine-structure" of neural firing density that may be useful for differentiation of normal and pathologic cochleae. The top panels show the mean numerical NDFs for the normal-hearing group in Experiment 1 and the bottom panels show the mean numerical NDFs for the normal-hearing and post-gentamicin groups compared in Experiment 2. Statistical analyses of the numerical NDFs were not completed for this study; although a visual examination of the plots above suggest that the numerical NDFs also support the hypotheses that high-level chirps trigger a broader spread of neural firing than high-level 2 kHz tonebursts and that OHC pathology does not significantly alter high-level NDFs.